INTERACTION OF A SIDE JET WITH A SUPERSONIC MAIN STREAM

M. V. MORKOVIN
C. A. PIERCE, JR.
C. E. CRAVEN

BULLETIN NO. 35 · SEPTEMBER 1952 · PRICE: $1.20

THE ENGINEERING RESEARCH INSTITUTE of the University of Michigan was established by the Board of Regents of the University in October, 1920, as the Department of Engineering Research. This action was taken on recommendation of representatives of Michigan industries and of the College of Engineering, who recognized that the University's facilities, both personnel and laboratory, could be advantageously used for industrial research. The wisdom of the Board of Regents in pioneering in the establishment of a department devoted to the promotion of industrial interests through sponsored research has been attested by the rapidly increasing demand for research services in the physical sciences as well as in engineering during the past thirty years.

Further information about the Institute may be obtained by requesting a copy of *Research in the Engineering and Physical Sciences, University of Michigan, Engineering Research Institute.*

For information relative to assistance on contemplated research projects, please address:

DIRECTOR, ENGINEERING RESEARCH INSTITUTE
University of Michigan
Ann Arbor, Michigan

A complete list of Institute publications will be found at the end of this brochure.

University of Michigan Press

UNIVERSITY OF MICHIGAN

ENGINEERING RESEARCH INSTITUTE

BULLETIN No. 35

Interaction of a Side Jet with a Supersonic Main Stream

INTERACTION OF A SIDE JET WITH A SUPERSONIC MAIN STREAM

M. V. MORKOVIN
C. A. PIERCE, JR.
C. E. CRAVEN

ENGINEERING RESEARCH INSTITUTE
UNIVERSITY OF MICHIGAN 1952

FOREWORD

This Engineering Research Institute Bulletin embodies the results of certain experiments conducted in 1950 in the University of Michigan Supersonic Wind Tunnel.

The authors wish to express their appreciation for the assistance given by the wind tunnel staff, especially Messrs. C. E. Wittliff, L. C. Garby, H. E. Bailey, and N. A. Fidh; to Mr. R. E. Phinney for preparing the preliminary copy for publication in the absence of the authors; and to the editorial staff of the Engineering Research Institute.

Financial support by the U.S. Air Force and by the Engineering Research Institute is also gratefully acknowledged.

Parts of the material in the present bulletin were used by the two junior authors in partial fulfillment of the requirements for their master's degrees at the University of Michigan.

M. V. Morkovin
C. A. Pierce, Jr.
C. E. Craven

SUMMARY

An experimental investigation was conducted in the University of Michigan Supersonic Wind Tunnel to explore the main characteristics of the flow and pressure field generated by a supersonic jet directed at 90° to the body into the 1.90-Mach-number tunnel stream. In particular, a study was made of the spreading characteristics of the jet and its gross effect on the normal force, drag, and moment of the cone-cylinder body, from which the jet issued. The phenomenon was investigated as a function of pressure ratio, p_0/p_s (jet stagnation pressure to tunnel static pressure), angle of attack of the body, and jet-nozzle geometry. Within a relatively short distance from the exit, the normal jet was turned in the direction parallel to the free stream even at pressure ratios of over 50. Simultaneously, it spread in all directions, mixing violently with the free stream. Optical evidence suggests that fringes of the jet are in contact with the cylinder. This may have practical implications for the use of hot side-control jets on bodies. The interaction resulted in regions of both high and low pressure over the body. The normal force on the body was decreased below the nominal jet side-thrust value, and the drag was increased above the no-jet value. A moment which depends on the geometry, particularly the length of the body, was generated about the nominal center of gravity of the body.

TABLE OF CONTENTS

LIST OF SYMBOLS

v_1	tunnel free-stream velocity (ft/sec)
p_1	tunnel static pressure (lb/ft^2)
ρ_1	tunnel air density (slugs/ft^3)
μ_1	tunnel absolute viscosity (slugs/ft-sec)
T_1	tunnel static temperature ($^\circ$R)
D	model maximum diameter (ft)
d	jet diameter at the throat (ft)
p_h	static pressure at any orifice on model (lb/ft^2)
p_0	jet stagnation pressure (lb/ft^2)
ρ_0	jet stagnation density (slugs/ft^3)
μ_j	jet absolute viscosity (slugs/ft-sec)
v_j	jet velocity at the throat (ft/sec)
T_0	jet stagnation temperature ($^\circ$R)
R	gas constant (ft^2/sec^2-$^\circ$R)
C_p	specific heat at constant pressure (ft^2/sec^2-$^\circ$R)
γ	ratio of specific heats
θ	angle around body, measured from top of body ($^\circ$)
m_j	mass flux from the jet (slugs/sec)
$C_{M_{CG}}$	moment coefficient about the center of gravity (assumed to be on the side-jet centerline)
C_N	normal force coefficient
C_L	lift coefficient

C_D drag coefficient

α angle of attack ($^\circ$)

q dynamic pressure (5.4 lb/in.^{2} in tunnel)

Subscripts:

1 tunnel free-stream conditions

0 jet stagnation conditions

j pertaining to jet

LIST OF FIGURES

INTRODUCTION

Many three-dimensional flow phenomena encountered in engineering practice are exceedingly complex and therefore not amenable to detailed theoretical or experimental investigations. To explain such a phenomenon, it is imperative to achieve, at the beginning, an over-all understanding, or picture, of the flow and to bracket the parameters governing the phenomenon. Studies of specific design characteristics and of their control are more likely to succeed on the basis of this understanding.

Visualization techniques, especially when backed by some quantitative measurements, are naturally suited to exploratory investigations of this type, and their extensive use is indicated. Yet, there seems to be a tendency on the part of many research workers to neglect these qualitative measurements, or "data." Descriptive reporting of phenomena is often frowned on as "unscientific." However, the engineer frequently has to make conclusions from "data" which do not fit the conditions of his problem. For such inference processes the qualitative understanding, or picture, furnishes the best guide.

The flow field studied in this report, by selected static-pressure measurements and various visualization techniques, is that associated with the perpendicular issuance of a supersonic jet into a supersonic stream flowing past the jet. The report presents the inferred picture of the flow and the pressure data and includes such information on associated experimental problems as might be useful for further studies.

In order to investigate the major features of the interaction of supersonic jets at 90°, two possible experimental configurations were considered. The first consisted of allowing a supersonic jet, having its exit flush with the tunnel wall of the test section, to issue perpendicularly into the stream of a supersonic wind tunnel. The second consisted of placing a body in the test section of a supersonic wind tunnel and allowing a supersonic jet, having its exit flush with the body surface, to issue perpendicularly into the stream. The second configuration was chosen for two reasons. First, the boundary-layer build-up along the body would be small, as compared to that with the first method (Reference 1). Second, the three-dimensional similarity of the configuration to a body which makes use of side-control jets in actual flight may have implications for practical application.

The complete range of parameters governing the interaction of supersonic jets could not possibly be covered in this study. Theoretical considerations and physical limitations of the facilities lead to concentration on two aspects of the phenomenon: (1) the spreading characteristics of the side jet, and (2) the effect of the side jet on the normal force, drag, and moment about the center of gravity (which was assumed on the centerline of the side jet). It was hoped that the chosen range of parameters would make the general findings applicable to problems where the spreading and mixing characteristics of the jet are of primary interest as well as to problems where the effect on body forces is important.

The experiments were conducted in April and September, 1950, in the University of Michigan Supersonic Wind Tunnel. The general facilities of this 8 by 13-inch blow-down tunnel are described in References 4 and 5.

DIMENSIONAL CONSIDERATIONS

In setting out to explore a new physical problem, it is desirable to determine, by proper application of dimensional analysis, all the major parameters which may govern the phenomenon. For the principal dependent variable, one may take the static pressure p_h at a representative location in the flow or on the body itself, e.g., at one of the pressure orifices. For a fixed geometry of nozzle, body, and stream at supercritical jet pressures, the dependent variable p_h is expected to be determined by the following twelve physical quantities (see Appendix):

$$p_h = f(p_1, \rho_1, v_1, \mu_1, \gamma_1, p_0, \rho_0, \mu_j, \gamma_j, d, D). \tag{1}$$

The number of fundamental units (dimensions) in Equation (1) is three, viz., mass, length, and time. According to Buckingham's π theorem (Reference 7), there must exist a functional relationship between $12 - 3 = 9$ nondimensional parameters formed from the 12 variables in Equation (1). One may write

$$\frac{p_h}{p_1} = g\left(\frac{p_0}{p_1}, \frac{\rho_0}{\rho_1}, \frac{v_1}{\sqrt{\gamma p_1/\rho_1}}, \frac{\rho_1 v_1 D}{\mu_1}, \frac{d}{D}, \frac{\mu_j}{\mu_1}, \gamma_1, \gamma_j\right). \tag{2}$$

This is not necessarily the only combination of dimensionless parameters that may be formed. However, any other such set of dimensionless numbers must be derivable from the one chosen here by multiplication or division with dimensionless numbers only. For example, the significant dimensionless parameter involving the relative mass flux in the jet and

stream, $[m_j/\frac{\pi}{4}\rho_1 D^2 v_1]$, could become an independent parameter if desired. The experimental control and direct measurement of such a mass-flux parameter, however, presented difficulties, so that it was not chosen as an independent parameter in the present analysis. Its dependence on the chosen parameters is as follows:

$$\frac{m_j}{\frac{\pi}{4}D^2\rho_1 v_1} = \left(\frac{d}{D}\right)^2 \sqrt{\frac{\gamma_j}{\gamma_1}\left(\frac{p_0}{p_1}\right)\frac{\rho_0}{\rho_1}} \left(\frac{v_1}{\sqrt{\gamma_1 p_1/\rho_1}}\right)^{-1} \left(\frac{2}{\gamma_j + 1}\right)^{(\gamma_j+1)/2(\gamma_j-1)} \tag{3}$$

When the jet gas is air, the parameter μ_j/μ_1 depends nondimensionally on T_0/T_1, i.e., on p_0/p_1 and ρ_0/ρ_1, and should be dropped:

$$\frac{p_h}{p_1} = h\left(\frac{p_0}{p_1}, \frac{\rho_0}{\rho_1}, \frac{v_1}{\sqrt{\gamma p_1/\rho_1}}, \frac{\rho_1 v_1 D}{\mu_1}, \frac{d}{D}, \gamma\right) . \tag{4}$$

In References 2 and 3, the dependence of flow coefficients and penetration of subcritical and mildly supercritical air jets issuing at 90° into a subsonic channel on the jet Reynolds number $\rho_j v_j d/\mu_j$, as in Equation (4), was reported. This dependence enters through the tunnel Reynolds number $\rho_1 v_1 D/\mu_1$ and the ratios p_0/p_1 and ρ_0/ρ_1.

Equation (4) exhibits a set of expected independent parameters governing air-jet interaction. Physical characteristics of experimental facilities further reduce the number of actually available independent parameters. Thus, in the present experiments, the parameters $v_1/\sqrt{\gamma p_1/\rho_1}$ and $\rho_1 v_1 D/\mu_1$, the Mach number, and the Reynolds number of the tunnel were fixed. More serious was the limitation on T_0/T_1, which forced ρ_0/ρ_1 to become nondimensionally dependent on p_0/p_1. To obtain appreciable variation of T_0/T_1, an impractically high jet temperature would be required. Before running the experiments, it was verified that T_0 varied at most 2°C as the pressure p_0 was varied from 100 psi to 40 psi. T_1 is the absolute atmospheric temperature in the tunnel bag (Reference 4), so that the ratio T_0/T_1 was essentially constant. The actual jet characterization was therefore merely through p_0 and d.

The above analysis holds for every geometric configuration of stream and body. Actually, two angles of attack were used, namely 0° and 14°. Hence, the investigation as planned can be summarized by the formula

$$\frac{p_h}{p_1} = f\left(\frac{p_0}{p_1}, \frac{d}{D}, \alpha\right) .$$

MODEL AND INSTRUMENTATION

The model consisted of a cone-cylinder combination, with a total cone angle of 20°, as shown in Fig. 1. Various dimensions of the model are shown in Fig. 2. This model was chosen for two reasons: first, because it was representative of the type of body in which a side-control jet might be used, and second, because experimental results of pressure distribution on this type of body, having the same cone angle, were available (Reference 9). The 2-inch diameter of the cylindrical portion of the body was selected to avoid the possibility of tunnel choking. In this connection it was feared that the side jet would add to the possibility of choking. Fortunately, no choking occurred, even when the jet was started before the tunnel.

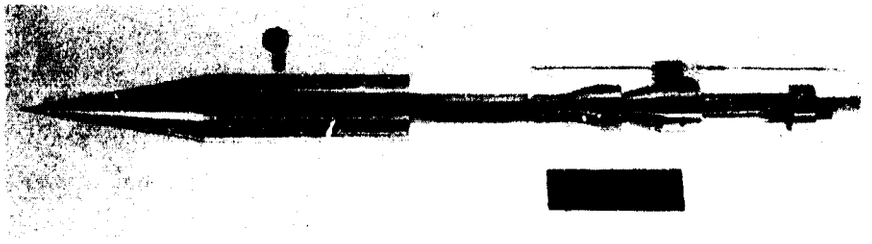

Fig. 1. Cone-cylinder model and nozzle piece.

It was decided to use a stagnation-pressure chamber and the total head probe in the model in order to obtain a direct measurement of p_0. This choice saved considerable work in obtaining p_0, as other methods considered involved accurate metering of the air and measurement of T_0, from which p_0 would then have to be calculated. (Unfortunately, the total head probe was damaged when additional experiments with steam and carbon dioxide were run in an attempt to determine more exactly the spread of the jet.)

Compressed air from a constant-pressure reservoir was fed into the body stagnation chamber through the sting, as shown in Fig. 3. The compressed air was controlled and regulated by a throttling valve in the air supply line to give variations in p_0 as desired. The air then issued through the nozzle into the supersonic stream of the tunnel.

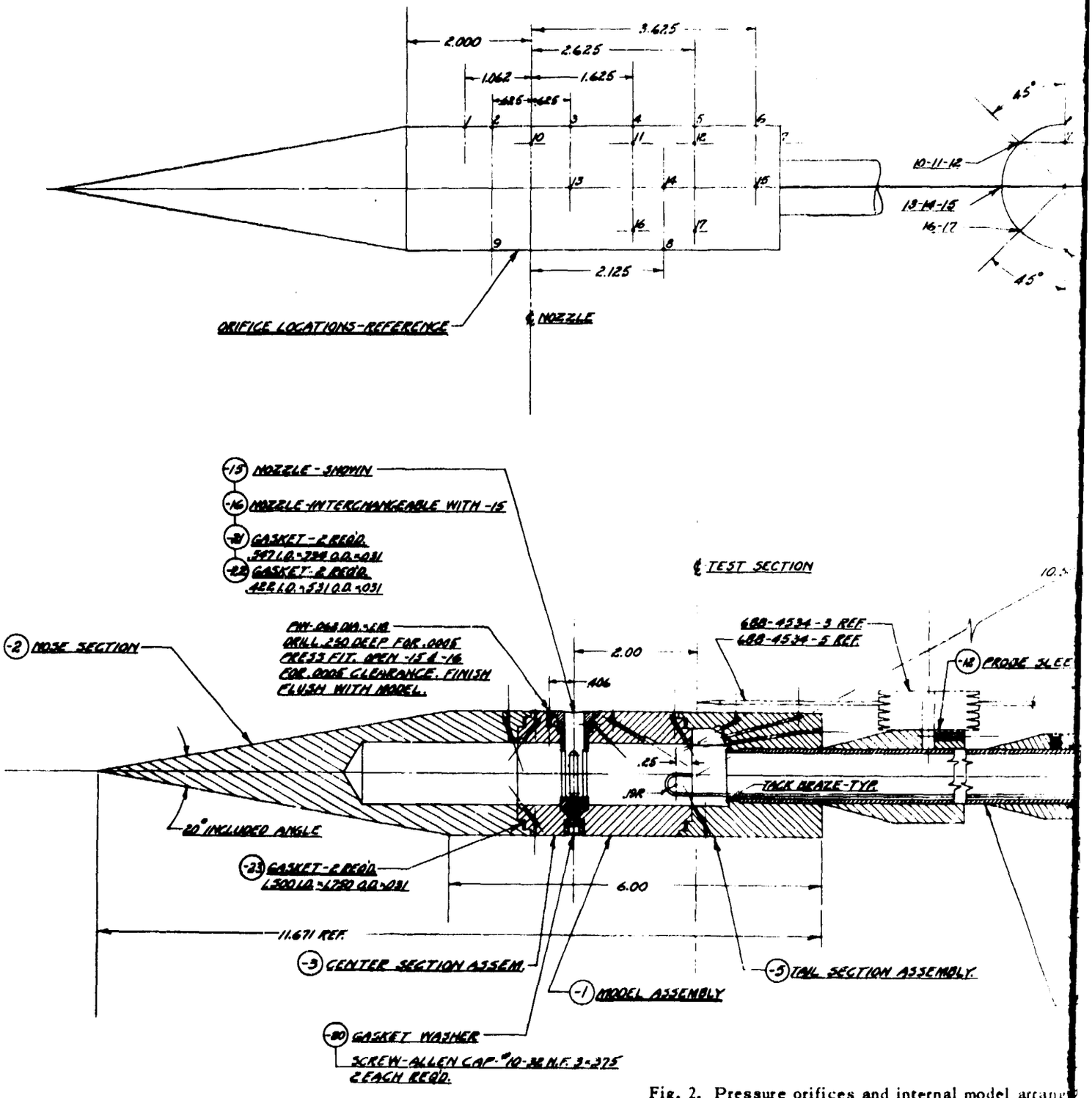

Fig. 2. Pressure orifices and internal model arrang

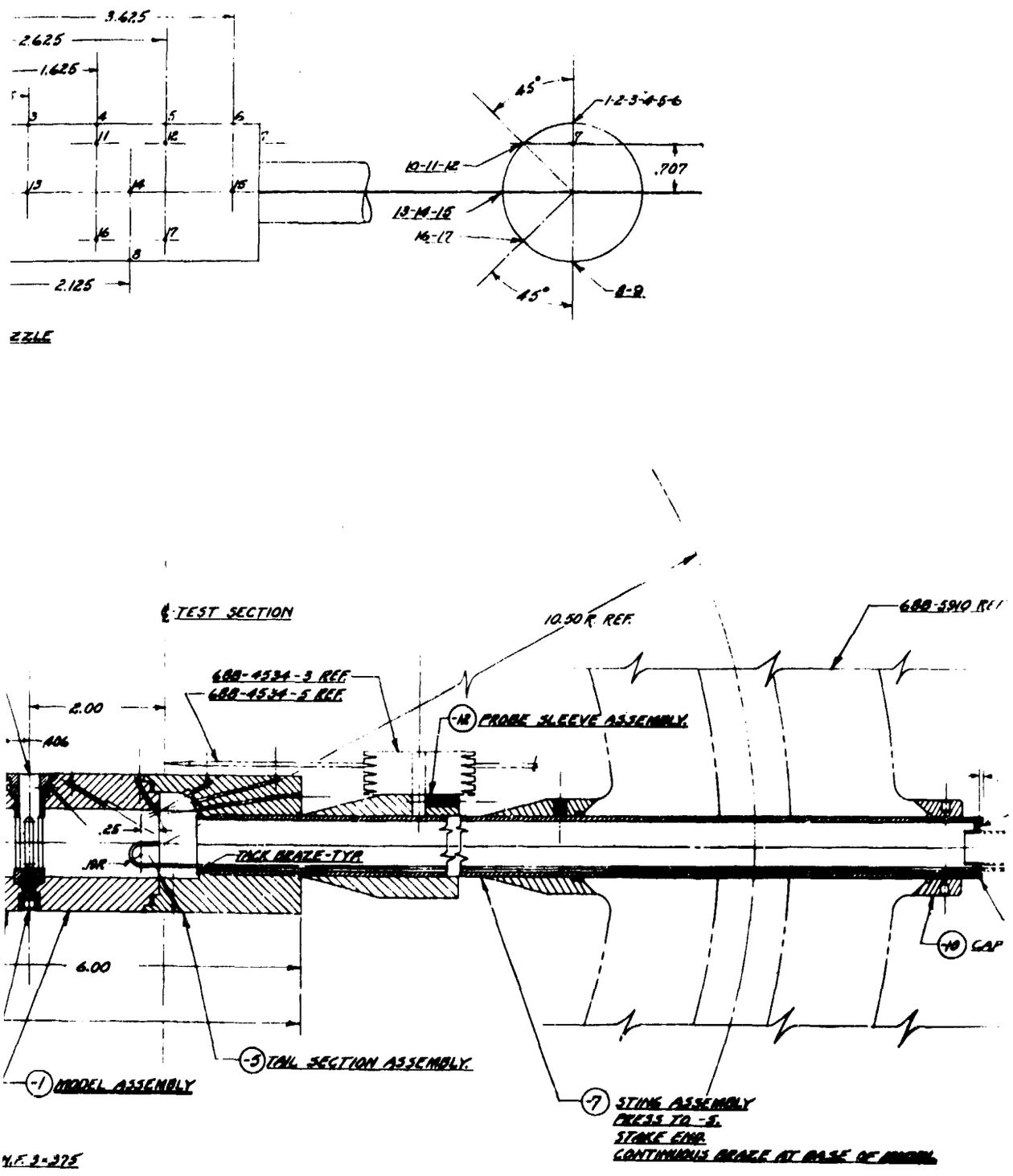

Fig. 2. Pressure orifices and internal model arrangement.

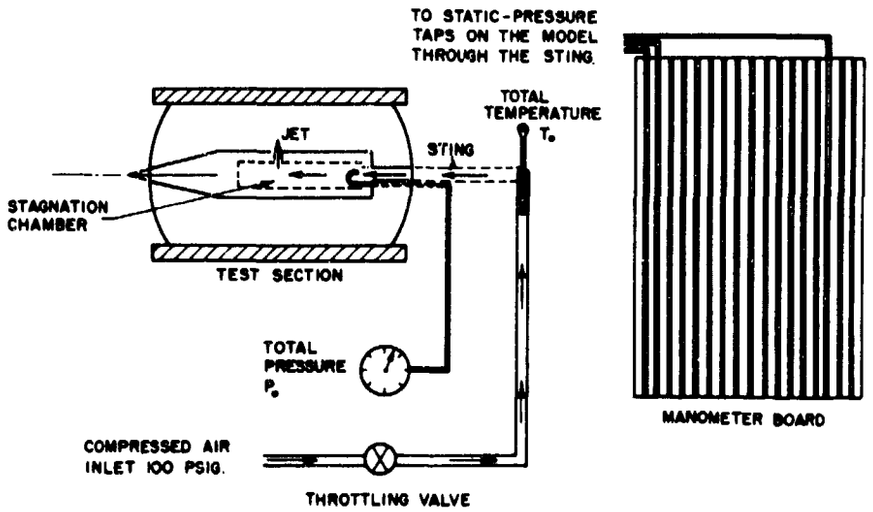

Fig. 3. Schematic test setup.

Two interchangeable side-jet nozzles were used. One nozzle was straight with a diameter of 0.32 inch; the other was a divergent nozzle with a throat diameter of 0.15 inch, an exit diameter of 0.32 inch, and a 15° divergence angle. An attempt was made to provide for the measurement of static pressure at the throats (Fig. 2). However, the complicated arrangement malfunctioned, so that a direct check on the critical pressure was not available. As the understanding of the interaction flow field increased during the experiments, it became clear that the small change in geometry from a straight to a divergent nozzle has a strong influence. It probably masks the functional dependence of the interaction field on the parameter d/D in Equation (4). As to dependence on α, the pressure runs were made only at $\alpha = 0°$ and $\alpha = 14°$ with the straight nozzle and at $\alpha = 14°$ with the divergent nozzle. The angle of attack of 14° was the greatest angle obtainable at the time; it was chosen in order to determine whether the side jet would tend to induce separation at high angles of attack. (Actually, a body on which a side jet would be used is more likely to fly at 0° or even negative angles of attack.)

Because of the complications of the model construction, only seventeen orifices in all were available; these were located in the region influenced by the jet (Fig. 2). It is clear that the interpolation between pressures so obtained cannot be very accurate. The estimates of the jet effects on the forces and moments calculated from the pressure distribution are indeed "gross," although they undoubtedly indicate correct trends. A

removable adjustable probe, used in other experiments, was available for investigations of static pressures at various locations near the model, as shown in Fig. 1. The mixing of the jet, however, was rather violent, so that the pressure probe indicated merely unsteadiness of flow in certain regions.

A schematic diagram of the location of the various instruments used is shown in Fig. 3. The pressure gage for measuring stagnation pressure in the model chamber was located beside the compressed-air-supply throttling valve to facilitate throttling to desired stagnation pressures, p_0. Stagnation temperature, T_0, was measured in the compressed-air supply line as close as possible to the model. This helped to minimize changes in stagnation temperature due to line losses in the air supply line. That portion of the air supply line exposed to the low temperatures in the tunnel was insulated with asbestos to prevent the low tunnel temperatures from affecting T_0. As a result of these precautions, stagnation temperature of the air supply was practically constant, at the point measured, throughout the experiment.

Static pressures from the seventeen static-pressure orifices were read on the manometer board, as shown in Fig. 3, to give values of p_h at various orifices. In addition, two static-flow pressures were read at points in the tunnel 14 inches upstream of the test-section centerline. These gave values of p_1.

DATA TAKING AND PROCESSING

The flow in the test section of the intermittent tunnel becomes steady 2 to 4 seconds after the opening of the butterfly valve leading to the low-pressure tanks (References 4 and 5), at which time the pressure leads are unclamped. The preset jet valve was opened approximately 1 second after the tunnel butterfly valve, so that, as a rule, the jet and the main flow stabilized within 5 to 6 seconds. Thus, an additional 14 to 15 seconds was available for the stabilization of the mercury levels in the manometer tubes. An observer watched the damping of the oscillations of the mercury and signaled for the photographic recording of the levels and for the shutting of jet and tunnel valves before the available time was up. Several runs had to be repeated because of obvious unsteadiness of the jet pressure, p_0 (especially at the lower p_0/p_1 ratios) or of the manometer levels. It has been the experience at the University of Michigan Supersonic Wind Tunnel that, if adequate precautions are taken, the pressures obtained by the procedure described are repeatable with a minimum of scatter,

TABLE I. STATIC-PRESSURE RATIOS ON BODY

Run No.	p_0/p_1	p_h/p_1 at Orifice No.:																
		1	2	3	4	5	6	7	10	11	12	13	14	15	16	17	9	8
$\alpha = 0°$, straight nozzle																		
4-21-1	0	.851	.900	.905	.945	1.000	1.025	.863	.920	.962	1.000	.933	1.075	1.15	.980	.960	.900	.977
4-21-2	0	.865	.935	.945	.995	1.050	1.083	.909	.958	1.017	1.059	.900	1.080	1.230	1.012	1.010	.950	1.033
4-22-6	28.3	1.041	1.230	.365	.665	1.167	1.359	.794	1.095	.860	.789	1.06	1.040	1.080	1.065	1.058	.920	1.009
4-22-4	29.9	1.069	1.309	.350	.546	1.180	1.140	.776	1.090	.845	.751	1.069	1.031	1.069	1.080	1.067	.932	1.007
4-22-3	33.05	1.078	1.324	.351	.532	1.239	1.455	.783	1.051	.847	.753	1.101	1.032	1.078	1.104	1.075	.930	1.028
4-22-8	40.2	1.071	1.320	.362	.523	1.272	1.514	.791	1.030	.840	.741	1.108	1.037	1.068	1.100	1.071	.938	1.070
4-22-7	47.0	1.080	1.309	.362	.543	1.156	1.579	.784	1.018	.825	.736	1.104	1.013	1.080	1.110	1.070	.919	1.019
4-22-2	48.8	1.080	1.280	.358	.484	1.150	1.624	.767	.949	.809	.705	1.113	1.001	1.049	1.120	1.086	.925	1.063
4-21-3	50.5	1.080	1.250	.354	.485	1.091	1.527	.755	.929	.805	.705	1.100	.999	1.041	1.100	1.067	.919	1.054
$\alpha = 14°$, straight nozzle																		
4-22-10	0	1.110	.935	.854	.950	1.110	1.327	.779	.861	.771	.883	.762	.789	.854	1.080	1.023	1.262	1.309
4-22-11	0	1.113	.866	.915	.980	1.077	1.292	.740	.800	.844	.894	.678	.725	.802	1.047	1.017	1.280	1.317
4-24-4	28.95	1.114	1.430	.411	.892	1.044	1.590	.683	.768	.665	.790	.965	.847	.880	1.070	1.070	1.309	1.340
4-24-6	31.70	1.090	1.470	.342	.773	1.102	1.598	.665	.720	.608	.747	1.000	.852	.883	1.050	1.046	1.282	1.320
4-22-13	44.6	.995	1.352	.414	.693	.948	1.660	.720	.741	.686	.734	1.064	.910	.888	1.058	1.063	1.290	1.325
4-22-14	45.1	.995	1.265	.344	.638	.865	1.698	.661	.698	.641	.694	1.081	.868	.855	1.045	1.073	1.271	1.284
4-22-16	48.1	1.007	1.430	.336	.668	.905	1.668	.670	.737	.605	.685	1.080	.885	.870	1.048	1.059	1.280	1.308
4-22-15	49.4	1.001	1.260	.346	.643	.825	1.644	.671	.725	.651	.720	1.077	.851	.854	1.049	1.074	1.278	1.306
4-22-2	51.0	1.126	1.412	.361	.632	.854	1.871	.826	.690	.652	.690	1.105	.879	.846	1.047	1.088	1.270	1.310
4-24-3	52.4	1.050	1.422	.338	.619	.805	1.753	.695	.689	.647	.695	1.118	.879	.850	1.054	1.098	1.280	1.321
4-24-17	53.0	1.111	1.210	.364	.645	.823	1.820	.725	.754	.675	.731	1.088	.889	.894	1.054	1.071	1.285	1.311
$\alpha = 14°$, divergent nozzle																		
4-22-10	0	1.110	.935	.854	.950	1.110	1.327	.779	.861	.871	.883	.762	.789	.854	1.080	1.023	1.262	1.309
4-22-11	0	1.113	.866	.915	.980	1.077	1.292	.740	.800	.844	.894	.678	.725	.802	1.047	1.017	1.280	1.317
4-24-13	27.45	1.135	.804	.563	1.021	1.085	1.548	.623	.926	.668	.858	.616	.616	.728	1.042	1.042	1.271	1.309
4-24-14	31.1	1.147	.825	.593	1.069	1.102	1.634	.664	.955	.695	.900	.638	.645	.750	1.021	1.021	1.281	1.320
4-24-11	44.0	1.122	.819	.454	1.020	1.099	1.80	.644	.976	.672	.851	.626	.642	.751	1.048	1.069	1.275	1.301
4-24-12	45.8	1.124	.825	.491	1.000	1.100	1.723	.651	.978	.656	.858	.631	.650	.775	1.050	1.070	1.280	1.311
4-24-8	56.9	1.105	.847	.442	.983	1.080	1.980	.628	.925	.630	.822	.634	.653	.817	1.050	1.080	1.278	1.308
4-24-9	57.5	1.105	.826	.430	.990	1.076	1.980	.624	.950	.636	.820	.620	.644	.811	1.047	1.076	1.275	1.308
4-24-15	58.7	1.120	.879	.444	.909	1.024	1.930	.667	1.002	.665	.907	.642	.699	1.028	1.048	1.080	1.311	1.317

and therefore are not influenced by the shortness of the run. The scatter in the present experiments was larger because of the additional stability problem of the jet itself; however, the accuracy is considered ample for the proposed study of over-all characteristics.

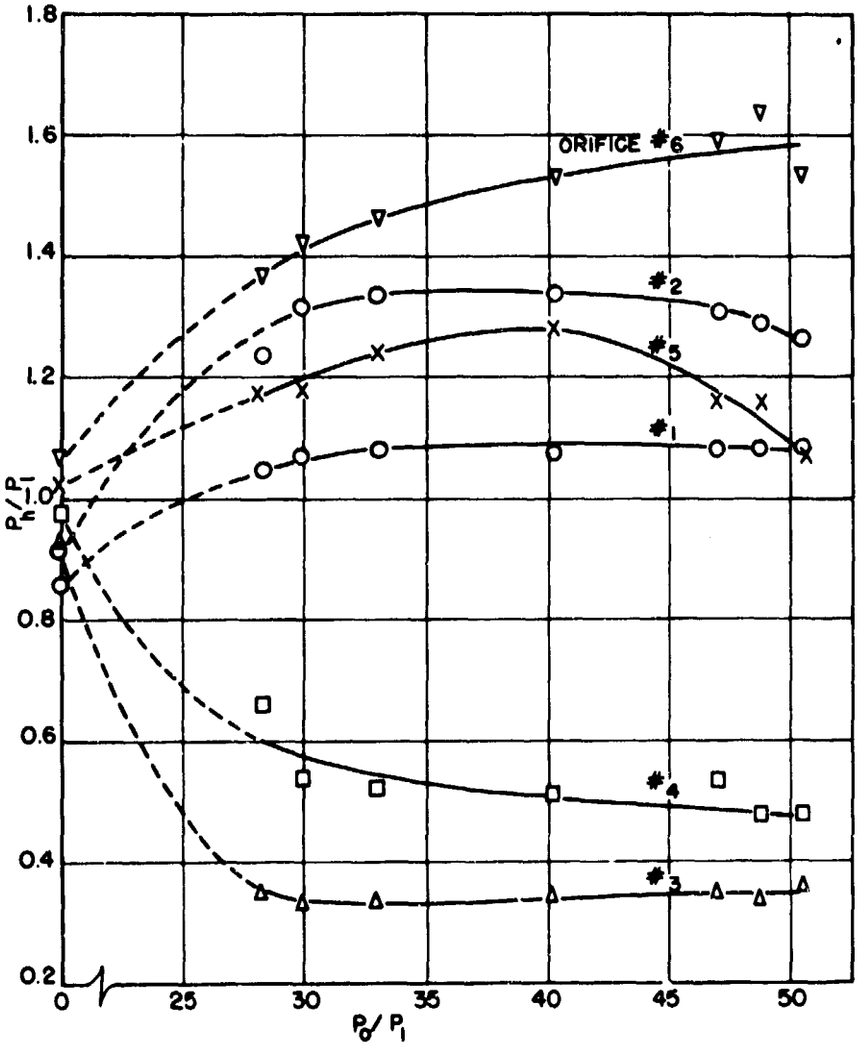

Fig. 4a.

Fig. 4. Variation of orifice pressure ratio, p_h/p_1, with jet total-pressure ratio, p_0/p_1; straight nozzle at $\alpha = 0^\circ$.

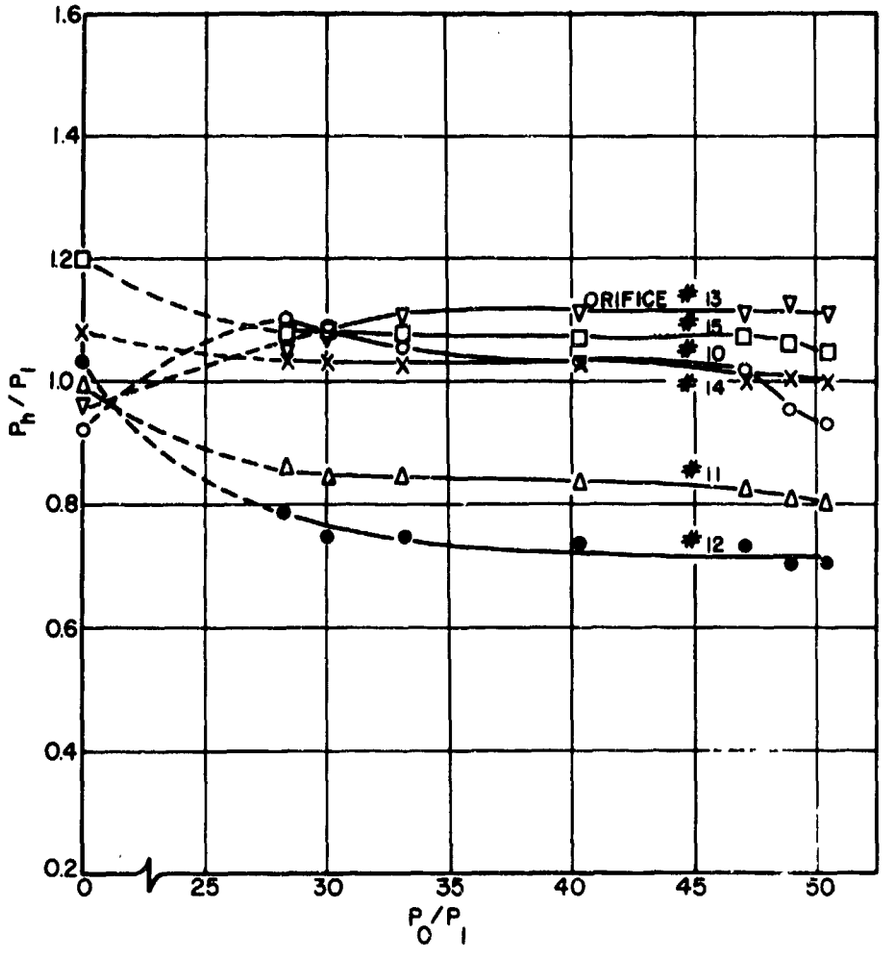

Fig. 4b.

The pressure data were processed in the usual manner (Reference 5) and are presented in Table I. Typical variations of all orifice pressures with the governing pressure ratio, p_0/p_1, are shown in Figs. 4a, b, and c for the straight nozzle with $\alpha = 0°$, and in Figs. 5 and 6 for the pressure orifices in the jet plane for both nozzles at $\alpha = 14°$. The pressure increments over no-jet values, $\Delta p_h/p_1$, were interpolated (and extrapolated) axially and circumferentially in the cases of maximum p_0/p_1, leading to a "probable overpressure surface." The affected area of the model was then divided into five 1-inch strips. For each strip, an axial overpressure

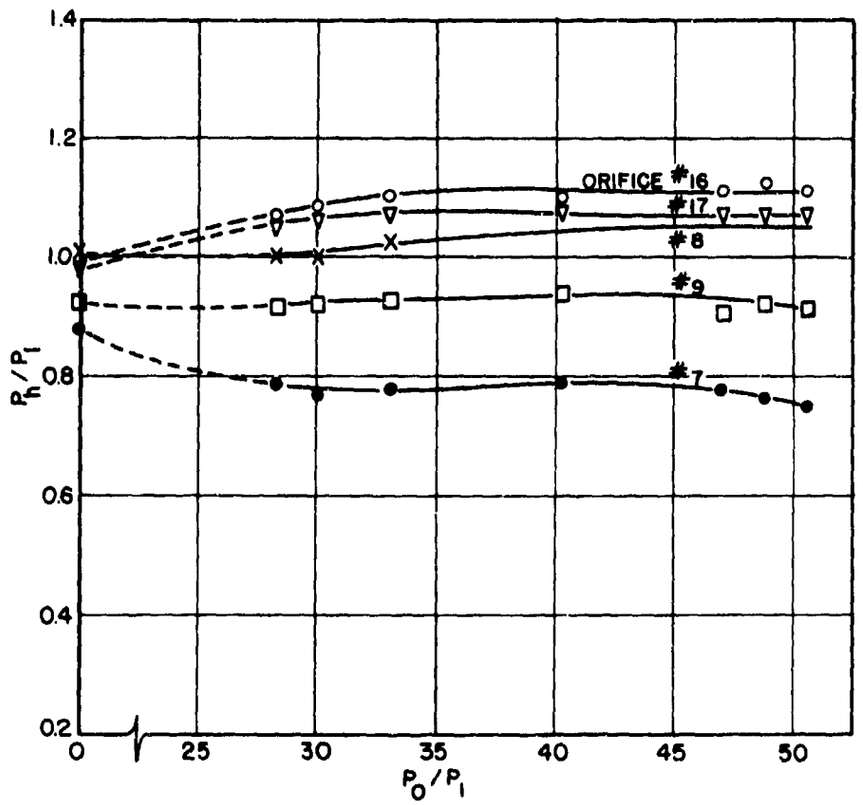

Fig. 4c.

average was estimated at nine equispaced meridional stations. Graphical integration of the vertical force components yielded the resultant "additional" force components and coefficients, as shown in Table II. The sectional additional force distributions for the straight nozzle at $\alpha = 0°$ can be seen in Fig. 7 for $p_0/p_1 = 50.5$.

During most pressure runs, schlieren photographs (with different knife-edge positions) were taken simultaneously with the photographs of the manometer board. Shadowgraphs, such as Fig. 8, were obtained later, as were schlieren photographs of a jet into a still tunnel, Figs. 9a and 9b. The vapor-light-scattering technique (first applied to supersonic investigations by NACA) was also used; Figs. 10a, 10b, and 10c display the patterns in cross-sectional planes, 1.56, 3.0, and 3.7 inches, respectively, aft of the centerline of the straight nozzle at $\alpha = 0°$ for a p_0/p_1 of 48. In an attempt to make the jet visible apart from the density pattern, steam, with p_0/p_1 approximately equal to 21, was blown through the straight nozzle

TABLE II

RESULTS OF INTEGRATION OF OVERPRESSURE DISTRIBUTION

Section	Normal Force, lbs.	C_N	Axial Force, lbs.	C_D	$C_{M_{CG}}$	C_L
$\alpha = 0°$, straight nozzle						
A	−.1309	−.0077				
B	.1922	.0113				
C	.288	.0170				
D	.205	.0121				
E	−.0471	−.0028				
Resultant	.518	.0306	0	0		.0306
On Base	.0231		.0231	.00136		
Moment					−.0277	
Total				.00136	−.0277	.0306
$\alpha = 14°$, straight nozzle						
A	−.149	−.0088				
B	.198	.0117				
C	.20	.0118				
D	.20	.0118				
E	−.1615	−.0095				
Resultant	.294	.0173		.0042		.0162
On Base	.0054		.0052	.00031		
Moment					−.0121	
Total				.0045	−.0121	.0162
$\alpha = 14°$, divergent nozzle						
A	.0265	.0016				
B	.137	.0081				
C	.087	.0051				
D	.050	.0029				
E	−.1922	−.0113				
Resultant	.1105	.0065		.0016		.0063
On Base	.0205		.0198	.00117		
Moment					.0107	
Total				.0028	.0107	.0063

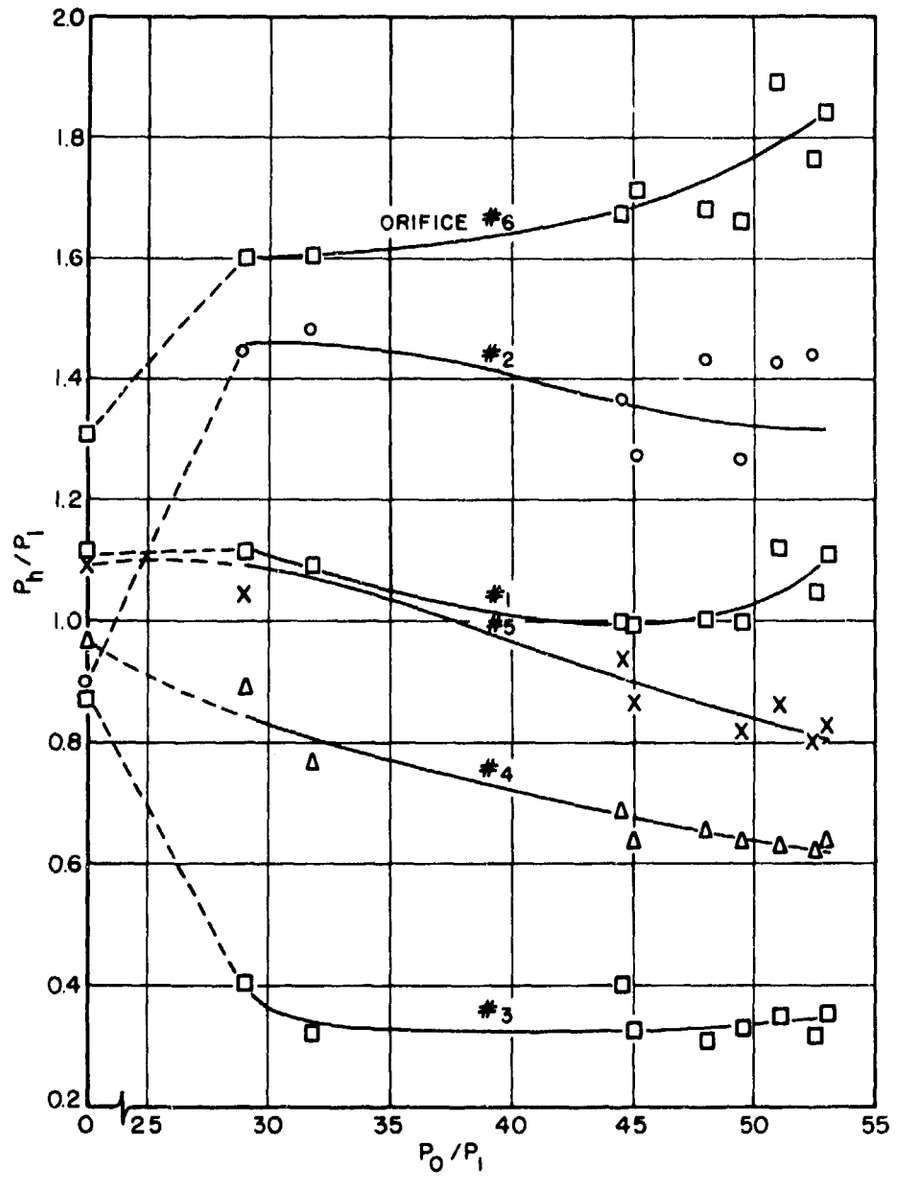

Fig. 5. Variation of top-orifice pressure ratio, p_h/p_1, with jet total-pressure ratio, p_0/p_1; straight nozzle at $\alpha = 14^\circ$.

(Figs. 11a and 11b). Comparison between Figs. 12a and 12b brings out the difference between schlieren photographs of steam and air at approximately

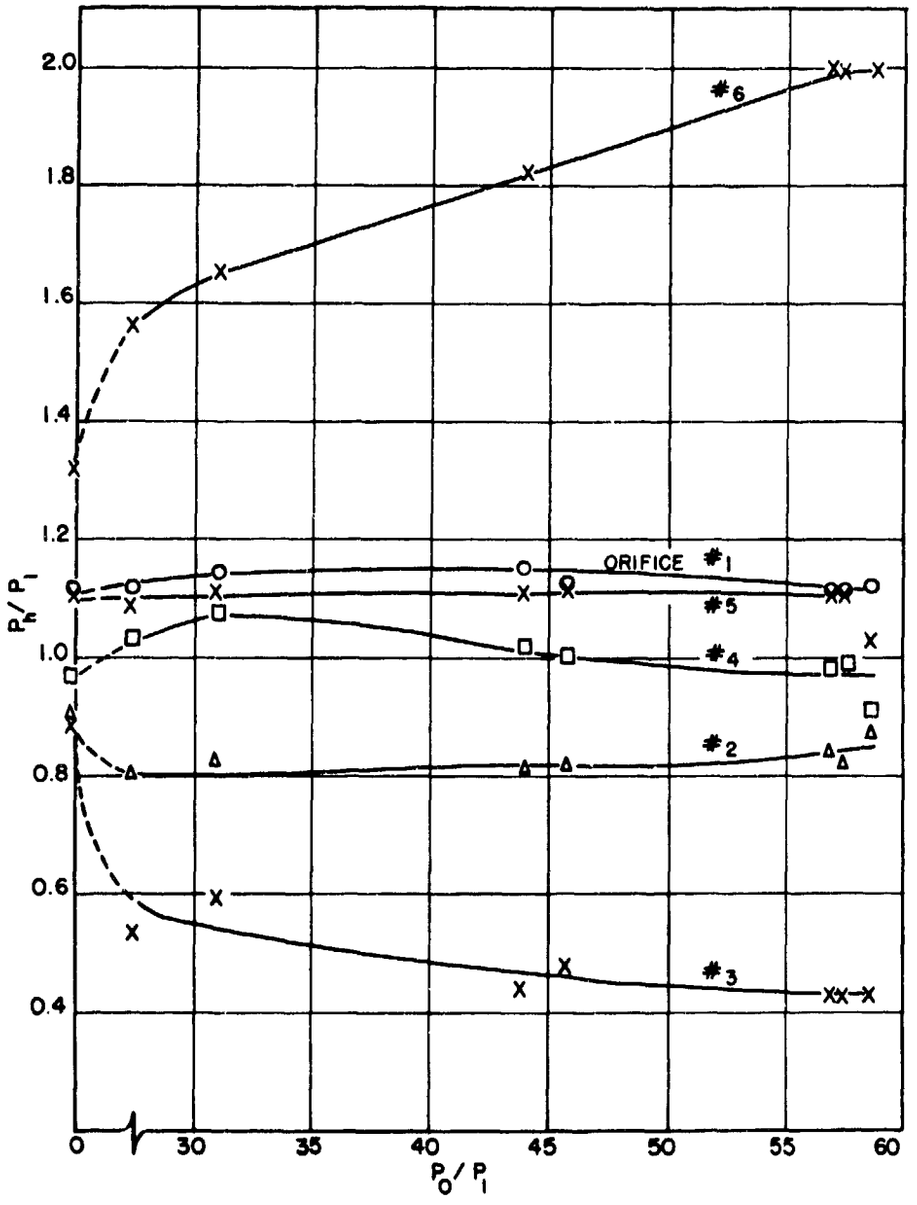

Fig. 6. Variation of top-orifice pressure ratio, p_h/p_1, with jet total-pressure ratio, p_0/p_1; divergent nozzle at $\alpha = 14^\circ$.

the same pressure ratio, $p_0/p_1 = 21$. Since the available steam pressure was relatively low, an attempt was made to adapt a carbon dioxide high-

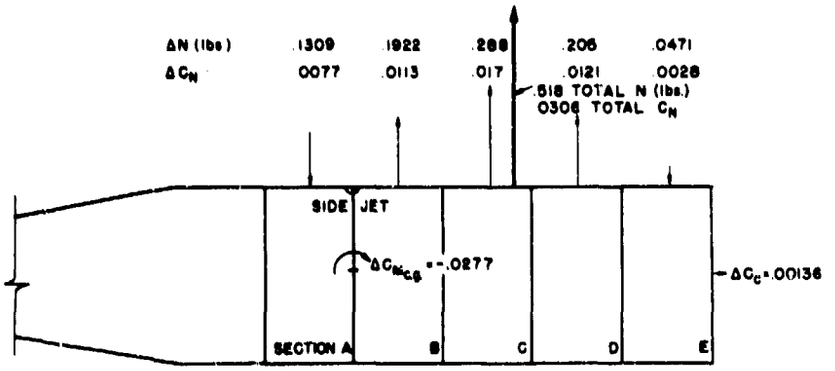

Fig. 7. Approximate force distribution due to pressure field induced by jet through straight nozzle at $p_0/p_1 = 50.5$.

Fig. 8. Straight-nozzle jet at $p_0/p_1 = 52.0$; shadowgraph; $\alpha = 14^\circ$.

pressure source to the system, but this was unsuccessful because of difficulties with line throttling.

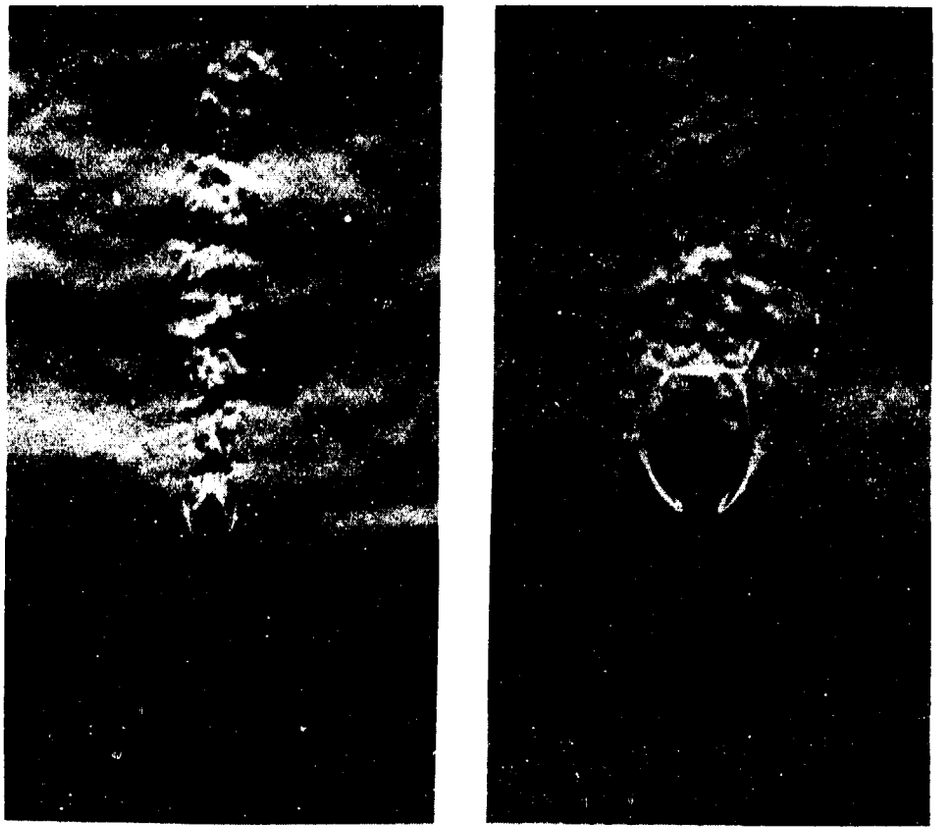

(a) (b)

Fig. 9. Jet flow into still air; $p_0/p_1 = 7$ and 56.

For visualization of streamlines in the inner portion of the boundary layer, the body was coated with a mixture of china clay and oil of wintergreen (Reference 14). During the run the liquid layer moves with the near-stagnant portions of the boundary layer toward lower-pressure regions and simultaneously evaporates, leaving clearly visible white lines on the surface. If the surface is blackened, photographs considerably superior to that reproduced as Fig. 13 (which is marred by reflections of light) can be obtained for a permanent record of the flow lines.

These patterns are very useful not only for qualitative appreciation of the boundary-layer flow but also for exact locations of even weak shock waves falling on the surfaces. In Fig. 13 the wet dark streak crossing obliquely from the bottom to the base of the body can be identified as the

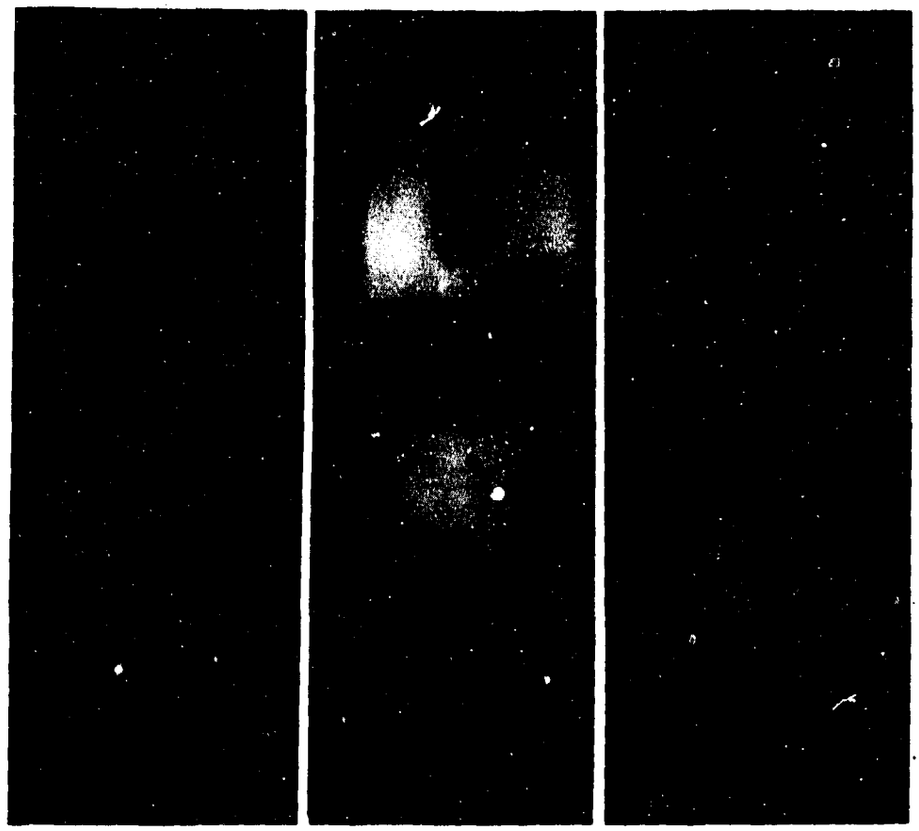

(a) (b) (c)

Fig. 10. Patterns of light scattering by moisture in the tunnel stream at plane sections 1.56, 3.0, and 3.7 inches aft of the jet nozzle axis; $p_0/p_1 = 48$; straight nozzle at $\alpha = 0^\circ$.

location of impingement of the shock inside the jet on the body (visible on schlieren photographs or shadowgraphs such as in Figs. 8 and 14). When the side jet was not operating, a small "kink" in the flow lines spread aft along a near-hyperbolic curve from a point on the side of the body, 1.3 inches forward of the base. This is the otherwise unobtainable line of impingement of the nose shock reflected from the side window back onto the rear part of the body. The reflection from the curved body is visible in Fig. 15, as discussed in Reference 10. Clearly, pressure orifice 15 is thereby affected, and to a lesser degree orifices 6 and 7, as is corroborated by Fig. 4. However, this reflected shock is not expected to

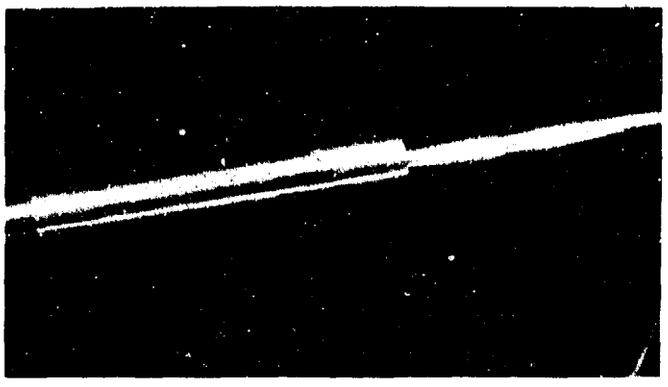

(a)

(b)

Fig. 11. Steam jet through straight nozzle at $p_0/p_1 = 21$, $\alpha = 10^\circ$; photograph and schlieren photograph 0.

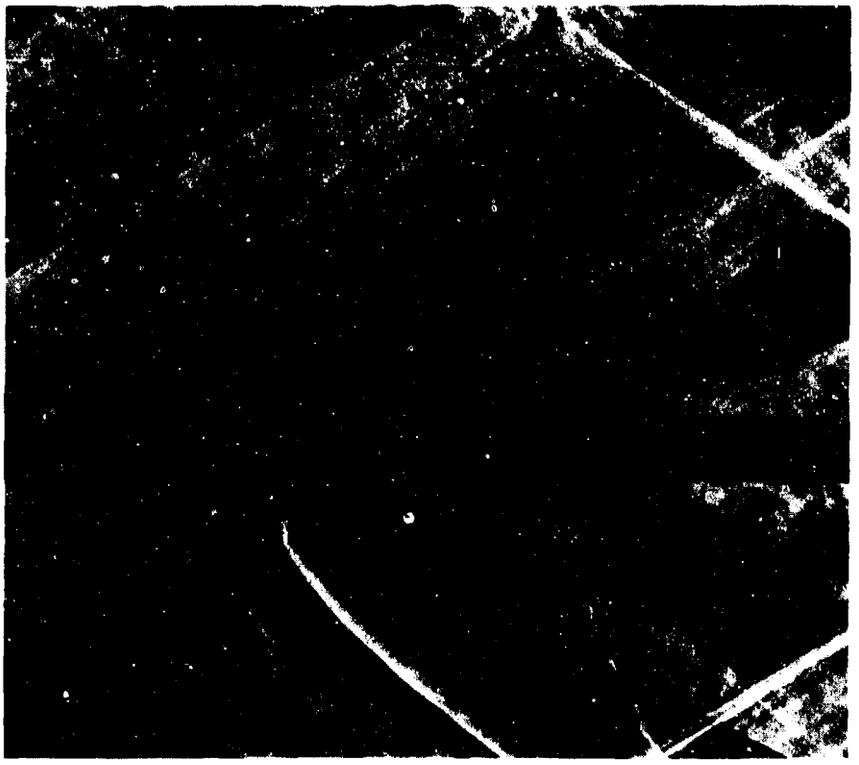

Fig. 12a. Jets through straight nozzle at $p_0/p_1 = 21$, $\alpha = 10^\circ$; steam and air.

influence appreciably the incremental pressures, Δp_h, which correspond to the actual jet interaction.

To obtain another qualitative indication of the flow, tufts were glued to the body in the affected areas. Also, a roughness ring was placed on the nose of the body to check on the effect of the nature of the boundary layer on the interaction field. This effect appears to be negligible except, perhaps, immediately upstream of the jet, where the laminar boundary layer separates farther forward of the detached shock in front of the jet than does the turbulent boundary layer.

JET MIXING AND PENETRATION

Already familiar is the shock and mixing pattern of a circular high-pressure jet issuing into the atmosphere, which has been studied in detail

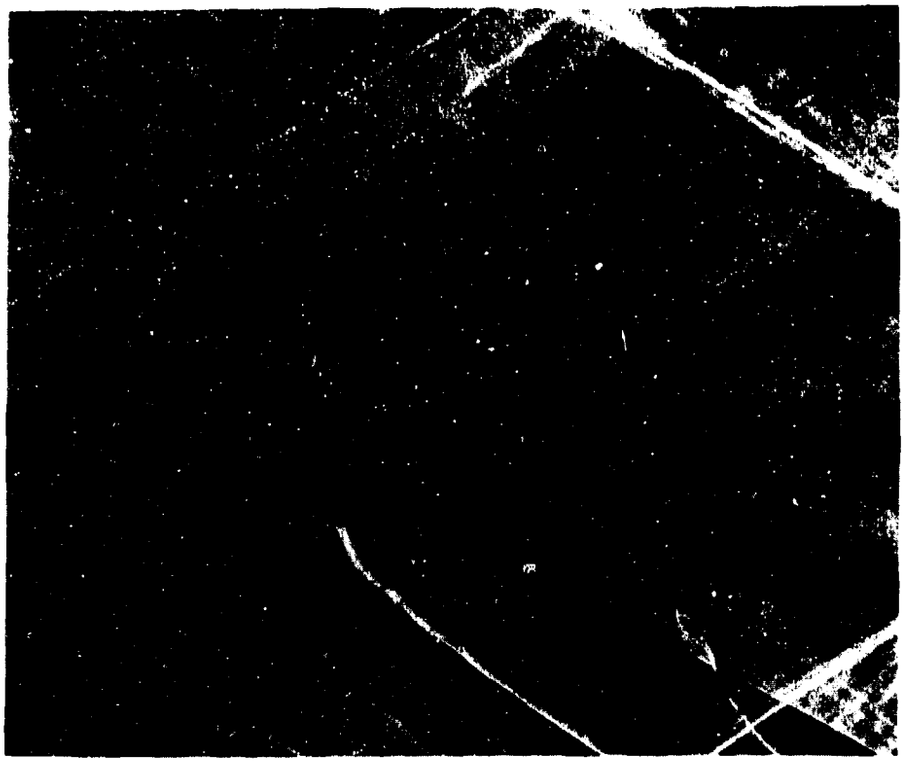

Fig. 12b. Jets through straight nozzle at $p_0/p_1 = 21$, $\alpha = 10^\circ$; steam and air.

by interferograms (Reference 11) and is shown here in Fig. 9a for the pressure ratio $p_0/p_a = 7$. The high-pressure jet air expands outward (black region in Fig. 9a) at the mouth to atmospheric pressure, p_a. However, the boundary of the jet cannot continue to diverge without overexpanding to subatmospheric pressures; the boundary, therefore, curves back, sending a gradual compression field (greyish region) toward the center of the jet, thus compensating for the increasing jet cross-sectional area. These pressure waves form an envelope type of shock (white line) focusing toward the jet axis. At high jet pressure, the converging shock wave cannot form a "regular intersection with itself," and a Mach Y intersection with the familiar normal shock meniscus results. The diverging portion of the Y shock reaches the boundary of the jet farther downstream and is reflected as an expansion wave fan (dark triangle), so that the

Fig. 13. Pattern of boundary-layer streamlines on the model.

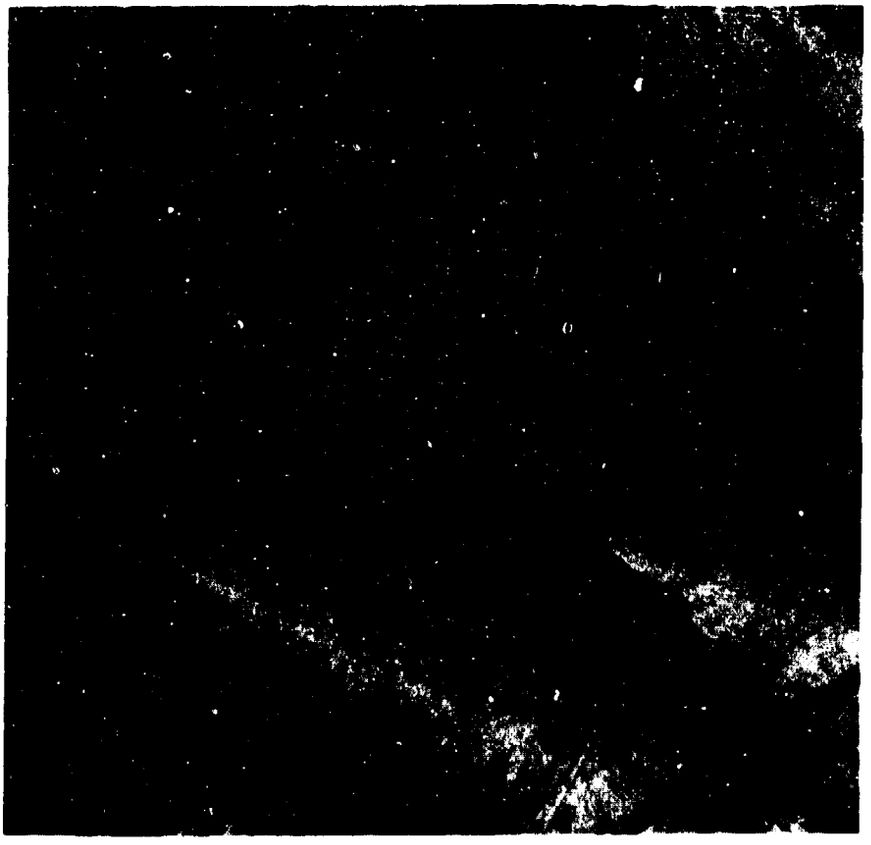

Fig. 14. Straight-nozzle jet at $p_0/p_1 = 48.8$; schlieren photograph 0; $\alpha = 0^\circ$.

boundary can remain at essentially the atmospheric pressure. The expansion-compression pattern continues to repeat itself in the jet with decreasing intensity, while the mixing at the boundary (jet-pump action) becomes turbulent and causes the reflections to be less and less distinct and pressures to depart from those obtainable by nonviscous theory.

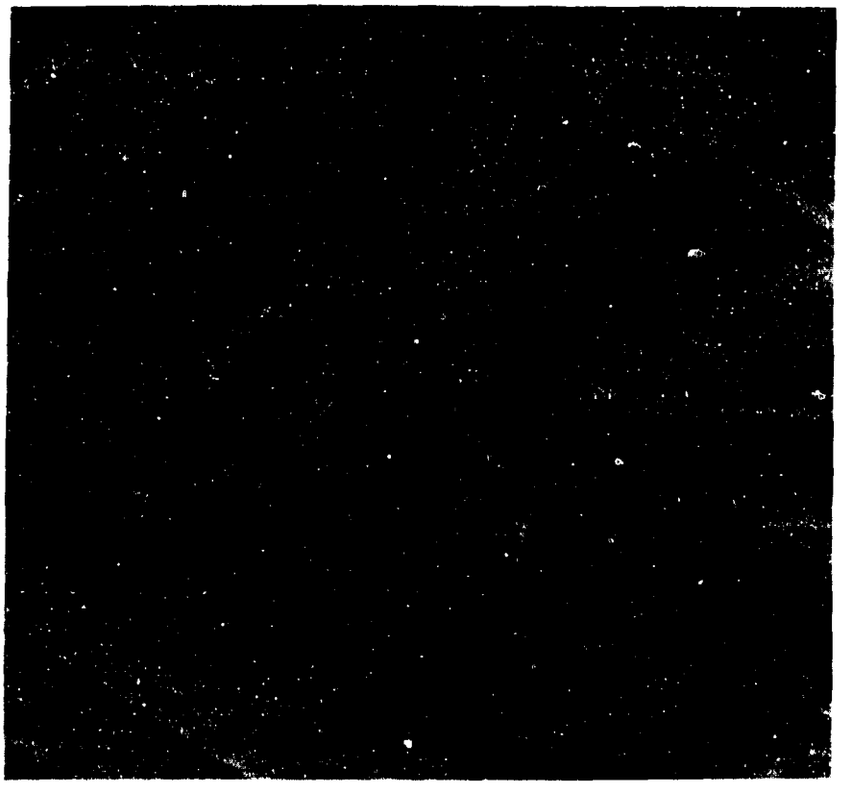

Fig. 15. No-jet schlieren photograph θ; $\alpha = 0^{\circ}$.

The understanding of the shock pattern in the jet gives a clue about the mixing region when the tunnel is operating. It is often not realized how the mixing increases and obliterates the reflection pattern when the pressure ratio across the nozzle increases. This can be seen in Fig. 9b, where $p_0/p_1 = 56$. Also to be noted are the increased angle of expansion at the mouth and the increased distance to the first meniscus.

Let us imagine for a moment the jet of Fig. 9a to be "frozen into a rigid column" while the supersonic tunnel flow is started. The obstruction would cause a detached shock upstream of the column, a highly accelerated flow around the sides of the column, a detached low-pressure wake with backflow in the vicinity of the rear of the column, and two stern shock waves with a higher-pressure region aft of the meniscus area of the wake. In the actual case, of course, horizontal momentum is imparted to the jet air column, which bends rapidly toward the direction of the free stream. The detached shock wave is present (Figs. 8 and 14) and so is the rapid

flow sideways around the obstruction, but the condition that the pressures in the tunnel air and jet air at the boundary of the bent column (when well defined) be equal undoubtedly distorts the boundary.

Mixing all around the jet, probably more violent than shown in Fig. 9b (and certainly more unpleasant to the ears of the observer), probably makes the distinction between jet air and tunnel air rapidly invalid. In particular, the low-pressure region of backflow of the "rigid column" appears to become a region of highly unsteady mixing. For a short distance (1 to 2 inches, depending on the pressure ratio) downstream from the jet exit, the flow seems to be directed downstream and away from the body, as judged from tufts and inferred from the boundary-layer flow pattern (Fig. 13). Farther downstream, as the diverging leg of the Y shock from inside the jet reaches the body and reflects (Figs. 8 and 14), the flow definitely follows the surface in this high-pressure zone. It is believed that the mixing in this "wake region" is such that "elements" of the jet air remain in contact with the surface of the body, and since the converging shock issuing from the rear of the nozzle exit must be inside the jet stream, the jet boundary, if it were clearly defined, would have to be almost tangent to the surface there (Figs. 8, 16, and 17). This belief is based on the following arguments:

(1) The mixing demonstrated in Fig. 9b is very strong, even without the low-pressure dead-air pocket. It is therefore very likely that mixed turbulent jet air remains at least intermittently in contact with the surface. Incidently, the distance of the meniscus from the jet exit seems not to be affected by the presence of the tunnel flow, although the area of the meniscus decreases.

(2) The diverging leg of the jet Y shock, although irregular and distorted, clearly reaches the body without any reflections as an expansion wave from any jet boundaries. This fact indicates that the air through which this shock passes cannot be separated from the jet air by any sharp discontinuity in density or velocity. If this air were a mixture of tunnel and jet air, even the irregularity of the diverging shock (and occasional appearance of two shock traces) would be consistent with the proposed explanation.

(3) Observation of a steam jet at a lower pressure ratio, approximately 21, indicated that steam adhered to the body surface and even appeared to cross the body base. Comparison of schlieren photographs of steam and air at this pressure ratio (Figs. 12a and 12b) appears to give conclusive evidence. Similar adhesion occurs even at $\alpha = 0°$, as Figs. 11a and 11b verify (although in this instance the eye was actually a more

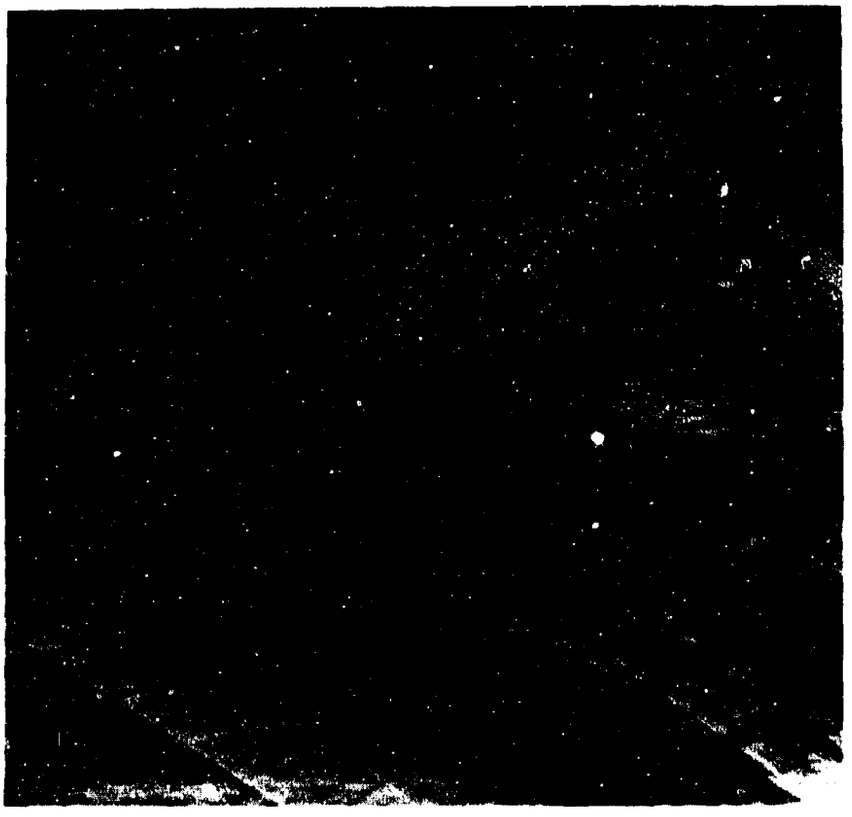

Fig. 16. Straight-nozzle jet at $p_0/p_1 = 47.3$; schlieren photograph 0; $\alpha = 0^\circ$.

discriminating instrument than the lens). At still lower pressure ratios, from 1.15 to 3.2, thermocouple probing of a hot jet issuing into a subsonic tunnel disclosed that near-maximum temperature existed at the wall; i.e., the jet air was in contact with the wall (Fig. 3 of Reference 1).

(4) The light-scattering pattern of Fig. 10a in a plane 1.56 inches aft of the nozzle centerline (5-second exposure) reveals a dark gray region near the surface, which is not inconsistent with the existence of a mixture region. The assumption is that the darkest zones correspond to the jet regions least contaminated by tunnel moisture particles. Patterns of Figs. 10b and 10c, 3.0 and 3.7 inches respectively downstream from the nozzle, could then be inte-preted as showing a contaminated, high-pressure region near the body and the formation of secondary flow in the jet core similar to that in curved pipes.

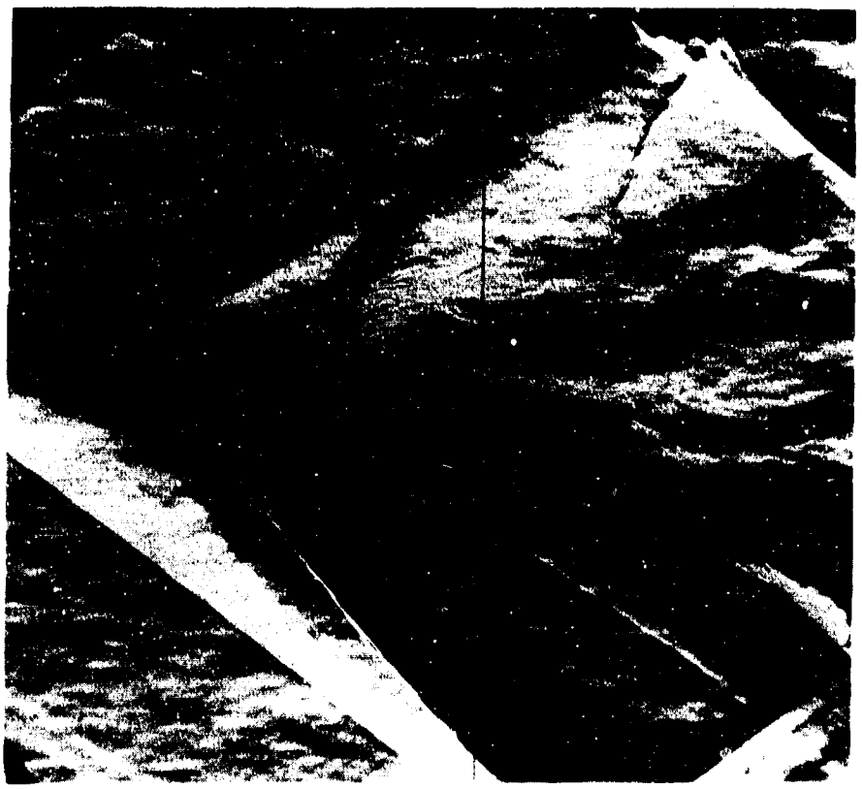

Fig. 17. Straight-nozzle jet at $p_0/p_1 = 53.0$; schlieren photograph θ; $\alpha = 14^\circ$.

Tuft studies corroborate that mixing occurs all around the jet, as already mentioned. Upstream of the jet nozzle, the detached jet shock causes gradual thickening and finally sudden separation of the boundary layer along the body, whether laminar or turbulent (Figs. 8 and 14). This separated air appears to be "pumped away" by the mixing with the boundary of the jet at the same rate as it forms.

Although the side jet seems to be a powerful mixing machine, the penetration of the jet into the supersonic stream is relatively small: at pressure ratios of over 50, its outer fringes pass between 2.5 and 3.0 inches away from the body at the base. This estimate is based on light-scattering patterns, shadowgraphs, schlieren photographs (to a lesser degree), and the interception of the weak tunnel-ceiling shock by the jet air. Sideways penetration is commensurately smaller; the partially vertical intersection of the detached jet shock with the side window (Figs. 14 and 16) and the

light-scattering patterns (Figs. 10b and 10c) indicate that the interaction is confined to a relatively narrow vertical (plume-like) region.

DISCUSSION OF THE PRESSURE RESULTS

The pressure information for the maximum pressure ratios, p_0/p_1, tested led to the integrated results of Table II, which are shown diagrammatically in Fig. 7 for the case of the straight nozzle at $\alpha = 0°$. The varied additional visual evidence led to the over-all picture of the flow and pressure field summarized in Fig. 18. Variation of pressure at specific orifices is shown in Figs. 4, 5, and 6.

Three general pressure zones due to the jet can be distinguished on the body (Fig. 18):

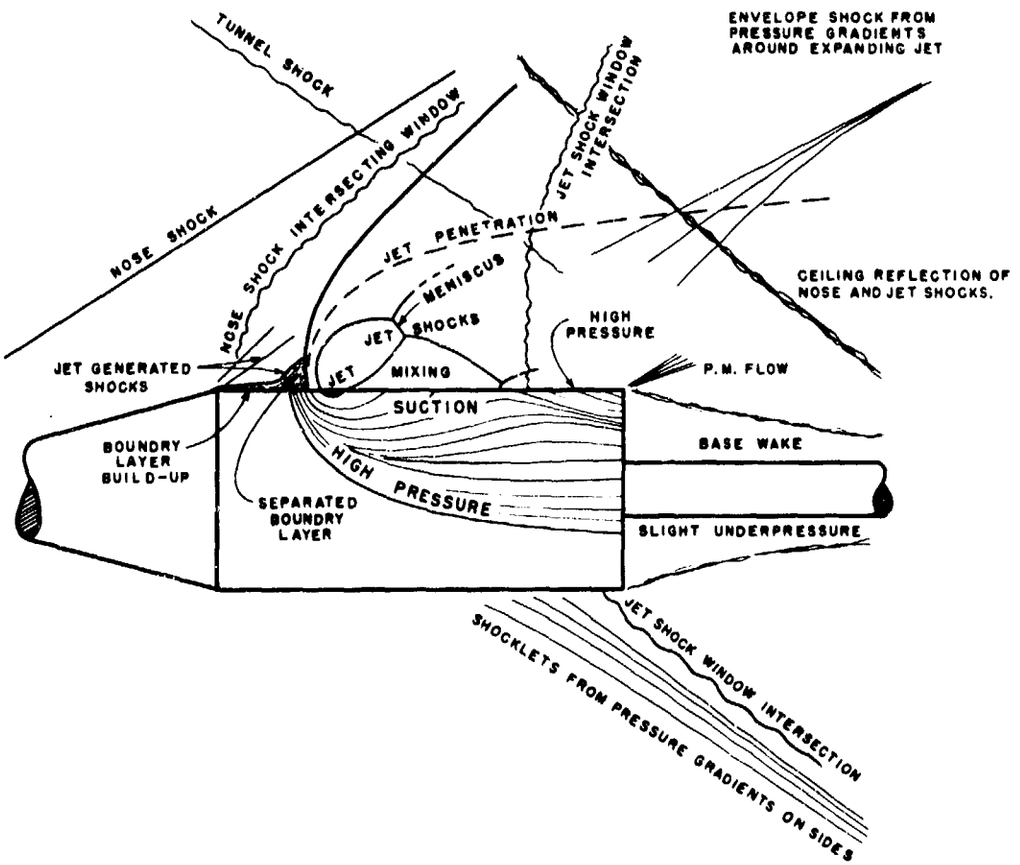

Fig. 18. Flow and pressure regions, from visualization techniques.

(1) There is a narrow band of high pressure on the outer edges of the area affected by the jet. This band is essentially the foot (trace) of the detached shock (in front of the jet column) rendered less sharp and wider through the boundary layer on the body. The patterns obtained by the evaporation technique (Fig. 13) indicate that the inner part of the boundary layer on the body is suddenly turned sideways and tends to flow along the high-pressure band; farther downstream this slow air gradually flows (fan-like) from the high-pressure band toward the low-pressure areas near orifices 4, 5, 11, and 12. It should be noted that the trace of the detached shock, and with it the high-pressure band, turns toward the free-stream direction faster than if the jet issued from a flat plate, because the curving of the surface shields the sides somewhat by preventing the direct influence along straight lines between any two surface points.

(2) Most of the surface, however, is in a low-pressure region, which is directly responsible for the decrease of the nominal thrust due to the jet. In the vicinity of the jet nozzle and in the "pocket" near orifices 4 and 5, the low pressure is caused primarily by the direct pump effect of the jet, as already discussed. The high acceleration of the flow around the jet obstacle is probably responsible for the formation of low-pressure zones farther away from the nozzle.

(3) The wedge-shaped high-pressure region at the rear of the body (dark lines in Fig. 13) could well counteract the decrease of thrust due to region (2), provided the body is long enough. This pressure region is partly associated with the return of the diverging leg of the Y shock inside the jet to the body, as already discussed. It is also associated with the flow around the jet obstruction; as the outer flow gradually straightens out after passing by the obstruction, compression waves are generated and a higher-pressure region results. The existence of such gradual compressive waves all around the jet is indicated by the wavelets which coalesce into an envelope-type shock as shown in the upper right-hand corner of Fig. 18. It is likely that the flow around the jet is not only straightened out but turned toward the "pocket," as in the case of flow around a rigid column. (This happens at least in the boundary layer; see Fig. 12.) In such a case stern shock waves would form, which could further account for the rather high pressure at orifice 6, especially in the case of the divergent nozzle.

It is clear that the magnitude of the "obstruction" to the tunnel flow due to the jet column should depend on the mass flux, m_j, in the jet (which for the straight nozzle and constant T_0 is proportional to the pressure ratio p_0/p_1). It appears that the various characteristic dimensions such

as the distance to the first jet meniscus, the distance to the high-pressure region on the rear part of the body, and the jet penetration increase almost linearly with m_j or p_0/p_1 in the range investigated. The variations of orifice pressure ratio, p_h/p_1, with p_0/p_1 given in Figs. 4, 5, and 6 can be understood by visualizing the spread of jet interaction pattern with increasing p_0/p_1.

The interaction field for the straight nozzle at $\alpha = 14°$ is basically little different from that at $\alpha = 0°$, and all the flow regions previously described are present (Figs. 8 and 17). There appears to be no tendency toward separation, even though in the absence of the jet the crossflow type of separation described by J. H. Allen (Reference 12) is in evidence downstream of orifice 5.

The shock pattern for the divergent nozzle at $\alpha = 14°$ (Fig. 19) is considerably more difficult to interpret. One must recall that at a given p_0/p_1

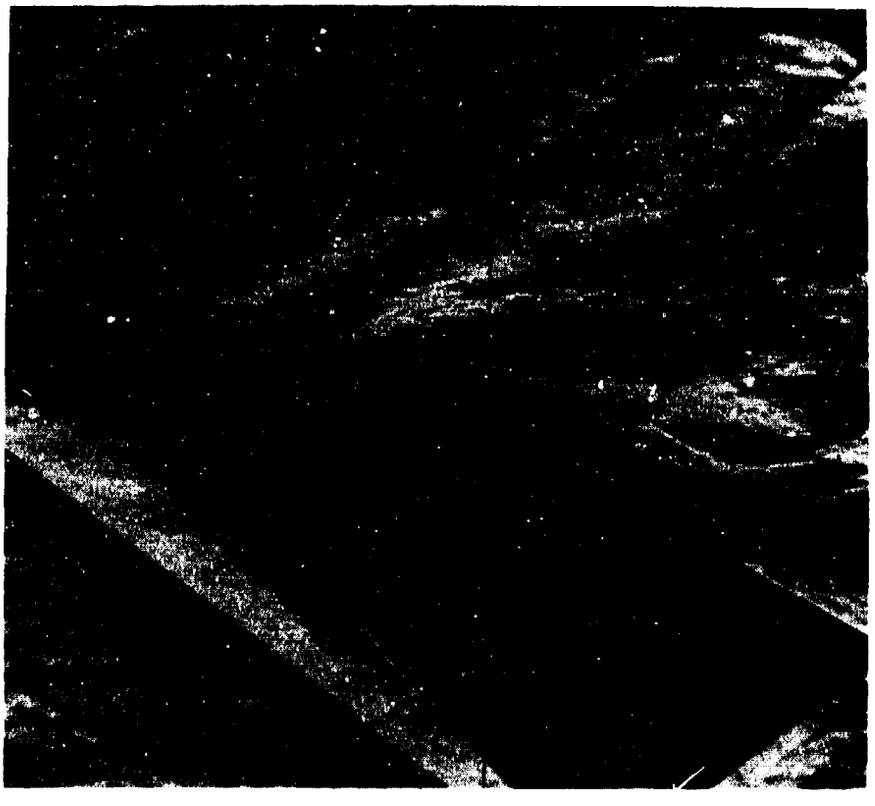

Fig. 19. Divergent-nozzle jet at $p_0/p_1 = 57.5$; schlieren photograph 0; $\alpha = 14°$.

value, the mass flux through the narrower divergent nozzle is slightly less than 25 percent of the mass flux through the straight nozzle. Furthermore, the 15° flaring of the nozzle allows considerable expansion of the jet within the body. The decreased obstruction of the tunnel flow (decreased jet flux) reduces the magnitude of the interaction field. In particular, it weakens the main jet-generated shock, lessens the upstream influence, including the extent of the separated boundary layer (see also effect on p at orifice 2), and decreases the jet penetration. The changed nozzle geometry modifies the flow near the jet exit and at the same time the pattern of the shock waves inside the jet. The shock surface originates at the rim of the nozzle and converges immediately toward the center of the jet; the intersection may be regular or of the Mach Y type, but with a very small meniscus. Examination of Fig. 19 discloses also two typical narrow dark lines nearly parallel to the body (i.e., forming angles of 50 to 60° with the shocks in the jet), which are believed to be associated with the flow around the jet stream. The envelope-type shock waves (upper right-hand corner of Fig. 18), also associated with the flow around the jet, are formed closer to the body than in the case of the straight nozzle. It is interesting to note that, even though the shock wave branch inside the jet which reaches the body surface with the straight nozzle is not in evidence, orifice 6 actually registers higher pressures than for the straight nozzle. This fact corroborates the theory that the rear high-pressure region is also associated with the flow around the jet and that it may have partly the character of the region downstream of the stern shock waves.

The change of the flow near the jet exit caused by the divergence of the nozzle can also be seen by the reversal of relative pressure values at orifices 2, 10, 13, and 14 (Fig. 2 and Table I). It would appear that the decreased obstruction of the jet narrows the pressure field in the vicinity of the nozzle "rimmed" by the high-pressure shock band, but that the flare of the nozzle widens the region of mixing and suction farther downstream, beyond orifices 13 and 14. The preceding interpretations are far from established; they are offered in order to exemplify how difficult it is to visualize the effect of the nozzle shape on the mixing phenomenon. It may be of interest that the phenomenon appeared to the observers to be steadier for the case of the divergent nozzle, resulting in a smaller scatter of pressure results than for a straight nozzle.

CONCLUDING REMARKS

The various visualization techniques, combined with the static-pressure measurements over the cylinder surface, yield a consistent picture

of the flow field generated by the supersonic side jet issuing perpendicularly into the supersonic main stream. The jet column bends rapidly downstream and remains relatively narrow despite the strong mixing all around the jet. Near the body surface, the bending appears to form a low-pressure pocket where the mixing is especially violent. It is likely that some of the air (gas) from the jet is kept in contact with the body through the mixing within this pocket (which may be important practically if the jet is hot). The pressure field due to the flow around the jet obstacle and to the jet-pump effect alters the forces and moments on the body, depending on body geometry, primarily length. In particular, the nominal side-jet thrust is decreased and the drag increased. The jet interaction is basically the same when the body is at an angle of attack and there is no tendency for the jet to induce separation or stall. For a given nozzle shape, the various lengths characterizing the interaction flow field appear to vary almost linearly with the mass flux in the jet for the range of pressure ratios investigated.

APPENDIX

PHYSICAL QUANTITIES RELEVANT TO SUPERSONIC JET MIXING

The real problem in the application of dimensional analysis to new phenomena concerns the a priori decision as to which physical quantities are relevant to the phenomenon. Buckingham (Reference 8) remarks that if the initial choice is in error, the conclusions of the analysis, which merely establish a certain constraint on the chosen quantities, will be in error. He states that the only test of the validity of the original choice lies in experimental verification. In complex cases, however, the success of the experiment and its interpretation depends to a considerable extent on the proper choice and minimization of the test parameters, i.e., indirectly on the conclusions drawn from the assumptions to be tested. Hence, an element of uncertainty usually persists until the problem has been subjected to repeated tests.

Often the local processes in the new problem can be described by locally valid equations which have yielded successful results in other problems. In such cases these equations provide additional confidence in the choice of the quantities relevant to the problem in toto even though the equations cannot be solved by available methods. Thus, the partial differential equations expressing the conservation of mass, momentum, and energy (Reference 13), together with the equation of state, give a reasonably well-proven description of the local flow of a homogeneous viscous heat-conducting compressible perfect gas. It is expected that these six equations will possess a field solution for the six dependent variables (not necessarily unique) which satisfies a suitable set of boundary conditions. The present problem of supersonic jet mixing should satisfy these equations locally, within the usually accepted idealization. The new feature of the problem is the increased complexity of the boundary conditions. The set of desired quantities is reached with a better appreciation of the inherent assumptions by examining the physical quantities of a parametric nature which occur in the differential equations and in the boundary conditions.

Equations	No.	Dependent Variables	Physical Quantities
Continuity	1	u, v, w, ρ	—
Energy	1	u, v, w, ρ, p, T	μ, k, C_p
Navier-Stokes	3	u, v, w, ρ, p	μ, g
State	1	ρ, p, T	R

It is convenient to consider $C_p T$ rather than T as a dependent variable, so that all "quantities" in the six equations are directly expressible in units of mass, length, and time. The equation of state, then, involves the ratio $R/C_p = (\gamma - 1)/\gamma$ (rather than R alone); and the energy equation the quantities μ and k/C_p. The solution of the set of six equations in six unknowns is expected to depend on the physical quantities directly present in these equations, namely, μ, k/C_p, γ, and g. If the gases in the main stream and the jet are different, the dependence will be on g, μ, $(k/C_p)_1$, and γ_1 and μ_j, $(k/C_p)_j$, and γ_j.

The boundary condition $v = 0$ over the body surface introduces no new physical quantities except D, which describes fully the boundary for a set of geometrically similar bodies. The condition of no heat transfer, $\partial(C_p T)/\partial n = 0$, which holds for steady-state flow, adds nothing. The free-stream conditions are completely specified by the physical quantities p_1, ρ_1, and v_1, which must therefore be added to the set. Additional parameters describing free-stream turbulence could be added; the intuitive expectation that the phenomenon is insensitive to these and similar parameters is supported by the finding of no appreciable influence due to changes in boundary layer over the body. The boundary conditions corresponding to the "free-stream conditions" in a supercritical jet can be described adequately by γ_j, the jet stagnation values p_0 and ρ_0 at the nozzle exit, and the boundary characteristic d.

Intuitive appreciation and experience with similar problems suggest that the flow will not be sensitive to the quantities g and μ/C_p, which would lead to Froude and Prandtl numbers, respectively. It is possible that some of the other physical quantities could be dropped as unimportant, but, in the absence of more definite information, it seems best to keep the present set of physical quantities on which u, v, w, ρ, p, C_p, and T may depend, namely p_1, ρ_1, v_1, μ_1, γ_1, p_0, ρ_0, μ_j, d, and D; see Equation (1).

In conclusion, it must be remarked that the characterization of the jet parameters is considerably more difficult if the jet is not homogeneous or involves changes of state or even chemical changes. The qualitative tests using steam in the jet disclosed no major influence of these additional factors.

REFERENCES

1. Callaghan, E. E., and Ruggeri, R. S., Investigation of the Penetration of an Air Jet Directed Perpendicularly to an Air Stream, NACA Tech. Note No. 1615, June, 1948.
2. Callaghan, E. E., and Bowden, D. T., Investigation of Flow Coefficient of Circular, Square, and Elliptical Orifices at High Pressure Ratios, NACA Tech. Note No. 1947, September, 1949.
3. Ruggeri, R. S., Callaghan, E. E., and Bowden, D. T., Penetration of Air Jets Issuing from Circular, Square, and Elliptical Orifices Directed Perpendicularly to an Air Stream, NACA Tech. Note No. 2019, February, 1950.
4. Garby, L. C., and Nelson, W. C., University of Michigan 8 x 13-inch Intermittent-Flow Supersonic Wind Tunnel, Univ. of Mich. Memo. No. 59, Engineering Research Institute, 1950.
5. Culbertson, P., Calibration Report on the University of Michigan Supersonic Wind Tunnel, Univ. of Mich. Memo. No. 36, Engineering Research Institute, 1949.
6. Pierce, C. A., Jr., and Craven, C. E., Investigation of the Effects of a Side-Control Jet on the Normal Force, Drag, and Moment of an Airborne Body in Supersonic Flight, Univ. of Mich. Wind-Tunnel Memo. No. 165, June, 1950.
7. Bridgman, P. W., *Dimensional Analysis*, Yale Univ. Press, 1931.
8. Buckingham, E., "Notes on the Method of Dimensions," *Phil. Mag.*, *42*, 696 (1921).
9. Dorrance, W. S., The Experimental and Theoretical Pressure Distribution and Normal Force of a Cone-Cylinder Configuration at a Mach Number of 1.9, Univ. of Mich. EMB-10, Engineering Research Institute, January, 1949.
10. Migotsky, E., and Morkovin, M. V., "Three-Dimensional Shock Wave Reflections," *Jour. Aero. Sciences*, *18*, No. 7, 484-9, 504 (1951).
11. Ladenburg, R., Van Voorhis, C. C., and Winckler, J., Interferometric Study of Supersonic Phenomena, Part I, NavOrd Report 69-46, April, 1946.
12. Allen, J. H., Pressure Distribution and Some Effects of Viscosity on Slender Inclined Bodies of Revolution, NACA Tech. Note No. 2044, March, 1950.

13. Goldstein, S., Editor, *Modern Developments in Fluid Dynamics*, Vol. II, Oxford Univ. Press, 1938, Eqs (1), (2), (4), and (16) of Chapter XIV, pp. 601-607.
14. Phinney, R. E., and Murphy, J. S., "Visualization of Boundary-Layer Flow," Engineering Research Institute, University of Michigan, August 30, 1951; reviewed in *Jour. Aero. Sciences, 18*, No. 11, 771 (1951).

Published by the Engineering Research Institute of the University of Michigan, Ann Arbor. Edited by B. A. Uhlendorf, Editor of Publications, Engineering Research Institute.

NOTE: Time will be saved if the price of the bulletin or circular is enclosed with the order. Checks should be made payable to the University of Michigan and forwarded to the Engineering Research Institute.

Bulletins

number

1. INVESTIGATION OF CHARCOAL AND COKE PIG IRONS.—*W. E. Jominy*. 27 pages. January, 1926. *Out of print.*
2. VOLUME CHANGES IN GYPSUM STRUCTURES DUE TO ATMOSPHERIC HUMIDITY.—*A. H. White*. 26 pages. February, 1926. Price: Fifty Cents.
3. THE NEUTRAL ZONE IN VENTILATION.—*J. E. Emswiler and W. C. Randall*. 26 pages. April, 1926. Price: Fifty Cents.
4. STAINLESS STEEL, A DIGEST WITH ABSTRACTS AND BIBLIOGRAPHY.—*Albert E. White and Claude L. Clark*. 82 pages. November, 1926. Price: Fifty Cents.
5. THE ELEMENTS OF METAL CUTTING.—*Orlan W. Boston*. 95 pages. December, 1926. Price: One Dollar.
6. A METHOD FOR PREDICTING DAYLIGHT FROM WINDOWS.—*H. H. Higbie and W. C. Randall*. 76 pages. January, 1927. Price: Fifty Cents.
7. THE RELATION OF MOTOR FUEL CHARACTERISTICS TO ENGINE PERFORMANCE.—*G. G. Brown*. 129 pages. May 1, 1927. Price: One Dollar.
8. A STUDY OF PATENTS DEALING WITH THE ELECTRODEPOSITION OF CHROMIUM.—*Richard Schneidewind*. 49 pages. April, 1928. Price: Fifty Cents.
9. A MANUAL OF FLIGHT TEST PROCEDURE.—*W. F. Gerhardt*. Revised by *L. V. Kerber*. 122 pages. December, 1927. Price: One Dollar.
10. A STUDY OF CHROMIUM PLATING.—*Richard Schneidewind*. 140 pages. September, 1928. Price: One Dollar. *Out of Print.*
11. THE STABILITY OF METALS AT ELEVATED TEMPERATURES.—*Albert E. White and Claude L. Clark*. 130 pages. November, 1928. Price: One Dollar.
12. APPLICATION OF TRIGONOMETRIC SERIES TO CABLE STRESS ANALYSIS IN SUSPENSION BRIDGES.—*George C. Priester*. 50 pages. March, 1929. Price: One Dollar.
13. A PRACTICAL METHOD FOR THE SELECTION OF FOUNDATIONS BASED ON FUNDAMENTAL RESEARCH IN SOIL MECHANICS.—*W. S. Housel*. 117 pages. October, 1929. Price: One Dollar. *Out of print.*
14. THE VOLATILITY OF MOTOR FUELS.—*G. G. Brown*. 299 pages. May, 1930. Price: One Dollar.
15. FORMATION AND PROPERTIES OF BOILER SCALE.—*E. P. Partridge*. 170 pages. June, 1930. Price: One Dollar.
16. THE SURFACE WATERS OF MICHIGAN.—*R. L. McNamee*. 318 pages. June, 1930. Price: One Dollar and Fifty Cents.
17. A RAPID METHOD FOR PREDICTING THE DISTRIBUTION OF DAYLIGHT IN BUILDINGS—*Waclaw Turner-Szymanowski*. 86 pages. January, 1931. Price: One Dollar.
18. THE SURFACE DECARBURIZATION OF STEEL AT HEAT-TREATING TEMPERATURES.—*W. E. Jominy*. 51 pages. March, 1931. Price: One Dollar.
19. THE DESIGN OF CAPACITOR MOTORS FOR BEST STARTING PERFORMANCE.—*Benj. F. Bailey*. 26 pages. April, 1931. Price: Fifty Cents.
20. AN ANEMOMETER FOR A STUDY OF WIND GUSTS.—*R. H. Sherlock and M. B. Stout*. 38 pages. May, 1931. Price: One Dollar.
21. THE INFLUENCE OF ATMOSPHERE AND TEMPERATURE ON THE BEHAVIOR OF STEEL IN FORGING FURNACES.—*D. W. Murphy and W. E. Jominy*. 150 pages. October, 1931. Price: One Dollar.

number

22. The Effect of the Products of Combustion on the Shrinkage of Metal in the Brass Industry.—*C. Upthegrove and A. J. Herzig.* 66 pages. December 1931. Price: One Dollar.
23. Heating Asphalt with Diphenyl Vapor.—*W. L. McCabe.* 76 pages. July 1932. Price: One Dollar.
24. The Malleabilization of White Cast Iron.—*R. Schneidewind and A. E. White.* 76 pages. August, 1933. Price: One Dollar.
25. Scaling of Steel at Heat-Treating Temperatures.—*C. Upthegrove.* 34 pages. Aug., 1933. Price: Fifty Cents.
26. Permissible Stress Range for Small Helical Springs.—*F. P. Zimmerli.* 135 pages. July, 1934. Price: One Dollar. *Out of print.*
27. The Properties of Metals at Elevated Temperatures.—*C. L. Clark and A. E. White.* 98 pages. March, 1936. Price: One Dollar.
28. A Study of Corrugated Fiberboard. The Effect of Adhesive on the Strength of Corrugated Board.—*D. W. McCready and D. L. Katz.* 42 pages. February, 1939 with Supplement, Sept., 1939. Price: One Dollar.
29. A Study of Flow Phenomena in the Wake of Smokestacks.—*R. H. Sherlock and E. A. Stalker.* 51 pages. March, 1941. Price: One Dollar.
30. Durability of Light Weight Steel Construction, Part I Effect of Copper and Other Alloys Upon the Atmospheric Corrosion of Steel.—*J. H. Cissel and W. E. Quinsey,* 70 pages. June, 1942. Price: One Dollar.
30. Durability of Light Weight Steel Construction, Part II A Study of the Service Records Light Weight Steel Construction.—*J. H. Cissel and W. E. Quinsey.* 45 pages. November, 1942. Price: One Dollar.
30. Durability of Light Weight Steel Construction, Part III—Protection of Steel Surfaces From Atmospheric Corrosion.—*J. H. Cissel and W. E. Quinsey.* 333 pages. November, 1942. Price: Two Dollars.
31. The Design and Construction of Pressure Relieving Systems. *Nels E. Sylvander and Donald L. Katz.* 147 pages. April, 1948. Price: Three Dollars.
32. The Development of Prismatic Glass Block and the Daylighting Laboratory.—*R. A. Boyd.* 96 pages. February, 1951. Price: One Dollar.
33. Two Monographs on Electrokinetics—I. Helmholtz: Studies of Electric Boundary Layers. II. Schmoluchowski: Electric Endosmosis and Streaming Currents. *Translated by Phil E. Bocquet.* October, 1951, iii, 159 pages. Price: Two Dollars.
34. A Theory of Psychological Scaling.—*Clyde H. Coombs.* vi, 94 pages. May, 1952. Price One Dollar and Seventy-five Cents.
35. Interaction of a Side Jet with a Supersonic Main Stream.—*M. V. Morkovin, C. A. Pierce, Jr., and C. E. Craven.* viii, 34 pages. September, 1952. Price: One Dollar and Twenty Cents.

Circulars

1. A Proposed Standard Procedure for Computing Flight-Test Climb Data.—*L. V. Kerber.* 6 pages. May, 1927. Price: Twenty-five Cents.
2. A Vapor-Pressure Chart for Hydrocarbons.—*Hal B. Coats and George Granger Brown.* 17 pages. December, 1928. Price: One Dollar.
3. Commercial Chromium Plating.—*Richard Schneidewind.* 60 pages. January, 1930. Price: Fifty Cents. *Out of print.*
4. The Value of Research to Industry.—*R. Perry Shorts.* 16 pages. July, 1930. *Out of print. A new brochure is available on request.*
5. University Research as an Aid to Industry. 49 pages. Revised August, 1938. No charge.
6. Engine Performance at High Compression Ratios.—*H. E. Zuck.* 31 pages. March, 1931. Price: Fifty Cents.

Reprints

number

1. ZEOLITE WATER TREATMENT IN A LARGE CENTRAL HEATING PLANT.—*Alfred H. White, J. H. Walker, Everett P. Partridge, Leo F. Collins.* 27 pages. July, 1927. Price: Fifty Cents.
2. MACHINABILITY OF METALS.—*Orlan W. Boston.* 47 pages. February, 1928. Price: Fifty Cents.
3. PROPERTIES OF FERROUS METALS AT ELEVATED TEMPERATURES.—*A. E. White and C. L. Clark.* 16 pages. February, 1928. Price: Fifty Cents.
4. A STUDY OF CENTRIFUGALLY-CAST PIPE (Metal-Mould Process) VERSUS SAND-CAST PIPE.—*F. N. Menefee and A. E. White.* 37 pages. August, 1928. Price: Fifty Cents. *Out of print.*
5. BAKING PRACTICE FOR OIL-SAND CORES.—*H. L. Campbell.* 5 pages. August, 1929. Price: Twenty-five Cents.
6. COMPARISON OF THE PHYSICAL PROPERTIES OF VARIOUS KINDS OF CAST-IRON PIPE.—*F. N. Menefee and A. E. White.* 40 pages. August, 1930. Price: Fifty Cents.
7. INFLUENCE OF TIME ON CREEP OF STEELS.—*A. E. White, C. L. Clark, R. L. Wilson.* 19 pages. October, 1935. Price: Fifty Cents.
8. DETERMINATION OF OXYGEN AND NITROGEN IN STEEL.—*John Chipman and M. L. Fontana.* 12 pages. April, 1936. Price: Fifty Cents.
9. INTERNAL STABILITY OF GRANULAR MATERIALS.—*William S. Housel.* 42 pages. January, 1937. Price: Fifty Cents.
10. THE DESIGN OF FLEXIBLE SURFACES.—*William S. Housel.* 20 pages. August, 1937. Price: Fifty Cents. *Out of print.*
11. APPLICATION OF SURFACE CHEMISTRY AND PHYSICS TO BITUMINOUS MIXTURES.—*N. W. McLeod.* 62 pages. March, 1938. Price: Fifty Cents.
12. EXPERIMENTAL SOIL-CEMENT STABILIZATION AT CHEBOYGAN, MICHIGAN.—*William S. Housel.* 26 pages. November, 1938. Price: Fifty Cents.
13. THE SHEARING RESISTANCE OF SOIL—ITS MEASUREMENT AND PRACTICAL SIGNIFICANCE.—*William S. Housel.* 12 pages. May, 1940. Price: Fifty Cents.
14. HEAT TRANSFER COEFFICIENTS IN GLASS EXCHANGERS.—*Alan S. Foust and T. J. Thompson.* 24 pages. December, 1940. Price: Fifty Cents.
15. INTERPRETATION OF TRIAXIAL COMPRESSION TESTS ON GRANULAR MIXTURES.—*William S. Housel.* 56 pages. December, 1950. Price: One Dollar.

Special Publications: Tables

TABLES OF LIGHT-SCATTERING FUNCTIONS FOR SPHERICAL PARTICLES.—*R. O. Gumprecht and C. M. Sliepcevich.* xvi, 574 pages, cloth-bound. September, 1951. Price: $6.50.

TABLES OF RICCATI BESSEL FUNCTIONS FOR LARGE ARGUMENTS AND ORDERS.—*R. O. Gumprecht and C. M. Sliepcevich.* xvi, 260 pages, cloth-bound. September, 1951. Price: $3.50.

TABLES OF FUNCTIONS OF FIRST AND SECOND PARTIAL DERIVATIVES OF LEGENDRE POLYNOMIALS.—*R. O. Gumprecht and C. M. Sliepcevich,* xii, 310 pages, cloth-bound. November, 1951. Price: $3.50.

Special Publications: Monographs

UNISTRUT SCHOOL CONSTRUCTION.—*C. Theodore Larson and Project Staff.* 68 pages. December, 1951. Free on request.

Current Annual Report of Engineering Research Institute Sent on Request.